

## RESPONSE TO REVIEWER COMMENTS

### Reviewer 1:

(1) page 1, line 24: what is meant by “ice edge dynamic distribution” – is it “(dynamic) ice edge variations”?

We agree with this remark and corrected this sentence.

(2) page 2, lines 1-2: “...based on surface roughness and other characteristics of the scene”. Surface roughness is an ice property but not a scene characteristic (like texture). What you probably mean is “...based on gray tone variations (caused by variations of the backscattered radar intensity) and other...”

We agree with this remark and corrected this sentence.

(3) page 2 lines 4-5: should be rephrased...”...and open water can have similar  $\sigma_0$ , depending on wind speed and direction...”

We corrected this sentence.

(4) page 2, line 7: “...image texture and OTHERS...” – one more example for “others”?

We agree with this remark and corrected this sentence.

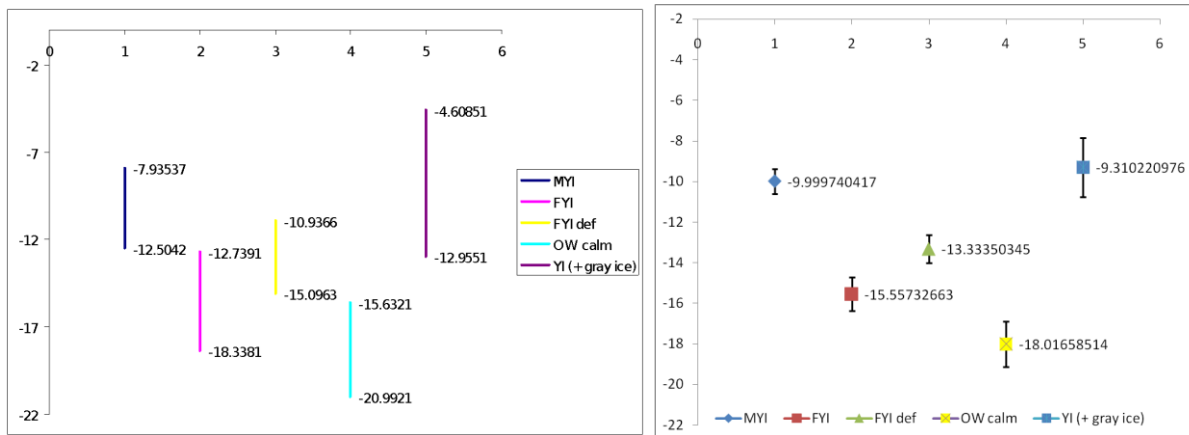
(5) page 2, lines 27-31: (a) It is not true that grey ice and multi-year ice show similar radar brightness at HH-polarization in any case – usually multi-year and first-year (level) ice can be very well distinguished at C-band HH-polarization. Only during summer the differences between young and old ice diminish.

(b) When does new ice appear bright? Usually it appears dark! The situations for a bright appearance that come into my mind are frost flowers or broken and deformed new ice (which due to deformation reveals a very rough surface).

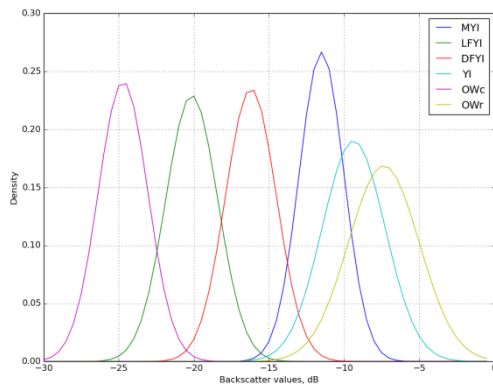
(c) At HV-polarization smooth thin ice appears dark, and open water appears dark as well, independent of the wind speed. The examples (a) – (c) have to be corrected and/or to be explained more in detail.

(a) We meant the young ice (gray and gray-white): young ice and MYI at HH-pol are rather similar, and, of course, they both are very well distinguished against level FYI. Young ice and multiyear ice show near similar brightness in the HH channel as the most similar in visual interpretation, we mentioned that their NRCS ranges are overlapped, but not the same.

We can illustrate what we mean: we have done some analysis for ENVISAT and RS2 data. For RS2 is not so satisfactory due to a few SAR data being in use for this analysis. The plots show the different sea ice types backscatter values, averaged in a 10 x 10 square samples, obtained from SAR images of ENVISAT (WSM, HH-pol) and RS2 (SCW, HH-pol).



Envisat ASAR WSM data(winter months, 2011), HH-pol, angular corrected at 31 deg: a) min and maximum of backscatter values, b) mean and STD of backscatter values



## 5 RS2 sigma0 distribution, winter 2012,2013, HH-pol, angular corrected at 35 deg.

We used term “young ice” following the WMO Nomenclature, and it includes grey (10-15 cm) and grey-white ice (15-30 cm). We understand that high backscatter of young ice (mostly grey ice) in the most (but not all) cases is due to complete coverage of its surface with frost flowers. According to Onstott (1992), the formation of frost flowers act to wick up brine and then form roughness elements on ice surface. An increase in surface roughness translates into an increase in backscatter. In some cases, high backscatter of young ice can be caused by its rafted/ridged to 100% surface. Wind-roughened open water also has high backscatter, which exceed that of young ice in many cases.

- 10 (b) Yes, we understand that new ice usually appears dark at HH and HV, and the sentence was written incorrectly. Affected by wind and surface currents the new ice sometimes forms a dense cluster, which has appearance the form of typical dark stripes and spots on the SAR images. These stripes and spots as the new ice (including *frazil ice*, *grease ice*, *slush* and *shuga*) has darker tone then rough OW, but in some case not so dark as level FYI \ fast ice or OW calm. We kept in mind the newer [younger] ice,
- 20 which with MYI is difficult to distinguish from sea ice (on different stages of development).

Our previous results showed that the NRCS values of grease ice obtained on ENVISAT ASAR images (HH-polarization, the 23° incidence angle) had range from -17.5 dB to -12.0 dB. In several other cases the NRCS values of grease ice amounted -7.43 dB and -6.15 dB at the start stage of its formation, while the NRCS values of the surrounding rough open water was about -4.0 dB. According to the study [Winebrenner D. P., Holt, E. D. Nelson. Observation of Autumn Freeze-up in the Beaufort and Chukchi Seas Using the ERS-1 Synthetic Aperture Radar , 1996] the backscatter of new ice can varied over the wide range - from -23 to -5 dB. Higher NRCS values can be explained by the possible presence of layered nilas, which backscatter is slightly higher than the smooth nilas [Atkinson P. M., A. R. L. Tatnall. Neural Networks in Remote Sensing, 1997].

(c) We agree that at HV-polarization smooth thin ice appears dark, and open water appears dark as well, independent of the wind speed. Here we mentioned that rough OW at HH-pol is rather bright since at HV-pol it is darker, that improves the OW distinguishing from sea ice.

We agree that these statements have some confusion information and corrected the text.

**(6) page 2, lines 31-34:** Does already the first sentence (“The dual polarization...”) refer to the work by Geldsetzer and Yackel, 2009, or to another study? [Geldsetzer and Yackel, 2009] use dual co-polarized C-band SAR imagery for discriminating sea ice types and open water during winter. The analysis was based on ENVISAT ASAR alternating vertical and horizontal polarization (VV, HH) medium-resolution imagery (from their paper).

**(7)** The goal of the present study is well described on page 3, lines 20-23. However, in my opinion it would be very useful if the authors emphasize the special motivation of their work, considering the fact that studies on classification with dual-polarization data were already published earlier.

We have included clarification of our motivation to the paper.

**(8) page 4, lines 6-8:** This is an important point of your work! You should emphasize here in addition that you have to analyze a larger number of radar images because the radar intensity contrast between open water and ice is varying significantly dependent on ice conditions and wind speed/direction (the latter affecting the radar brightness of open water).

We have included clarification to the paper: The radar images include the most typical samples since the radar intensity contrast between open water and ice varies greatly with ice conditions and wind speed/direction which significantly affect the radar brightness of open water.

**(9) page 4, lines 13-14:** Sentence: “The reason is...” I recommend discarding this sentence. Actually, the magnitude of the received cross-polarized signal depends on the structure of the illuminated target. In case of sea ice, e. g., the cross-polarized return increases with increasing macroscopic ice deformation.

We have discarded the sentence, since it was confusing.

**(10) page 4, lines 14-16:** “This causes...” Does the low intensity at HV-polarization explain its variation in across-track direction? I don’t think so. I guess the reason is technical limitations of the radar sensor electronics when

operated close to their noise level. Please check the Radarsat-2 manual. A good description of the HV-variations can also be found in Komarov & Barber, TGRS, Vol. 52, No. 1, pp. 121-136, 2014.

The next sentence was rewritten as follows: The HV channel includes disturbances in azimuth direction (visible as bright and dark stripes) along the burst boundaries in the ScanSAR Wide Beam SAR image (Fig. 2b).

**(11) page 4, line 22:** start “Our AUTOMATED...” Your automated algorithm does not include 6 steps but only 3 as you yourself explain on top of page 5. What you describe following this sentence is the first step of your analysis, namely the (manual) determination of thresholds and suitable textural measures that are later used in the fully automated (unsupervised) classification. Please formally separate the training/test part and the subsequent automatic classification more clearly.

We agree that the word ‘automated’ was not unambiguously describing the nature of the algorithm. Nevertheless, the algorithm is from the family of ‘supervised classification algorithms’ which are commonly understood to include both manual and automatic steps [e.g. Mohri, 2012]. We, therefore, believe that our algorithm also include all 6 steps - 2 of them are manual steps and are performed only one (2 - manual classification, 4 - training of the classifier), other steps are fully automatic. The word ‘automated’ was replaced with ‘semiautomatic’.

**(12) page 4, line 29-30:** Do you mean “Training of the automatic classifier (e. g. SVM) using different combinations of texture features together with radar intensity, based on manually classified images”? (is it really a “training” or rather a determination of thresholds between ice and water?)

It is actually a 'training' (also called 'machine learning'). At the training step (4) a ‘teacher’ provides values of texture features manually grouped in classes (e.g. ice, water, etc) to the SVM algorithm [BURGES, 1998]. This algorithm creates a hyperplane for categorizing values of TF. These hyperplanes (defined as polynomial coefficient values) are saved after training and are applied at the step (5).

**(13) page 5, line 5:** how large is the sliding window? (You can give a hint to section 3.4 in which you mention the sizes).

We have added: The image size .... window with 16 pixels step size (the detailed parameters are described in Sec. 4.2).

**(14) section 3.1:** I recommend that you provide the equation used for the incidence angle corrections and define the “linear-trend coefficient” that you use later. You should also give a hint that you discuss problems with this correction in section 5.1.

We included the equation with some description and hint.

**(15) page 5, line 24:** “incontinuity” = discontinuity? Since the problematic zones are masked out in the HV-images, one should also see them in the figures that you present later. But masks are not included in the figures.

The masks were excluded from the result images – this is a part of the algorithm.

**(16) page 6, sentence lines 2-4:** I assume that all co-authors understood this sentence but I do not. "...trained classifier..." = ice analyst from Met. Norge? If the images show, e. g., cracks, ridges and leads, why can't the "trained classifier" not identify them (they are distinct features)?

We slightly corrected this paragraph: ..... The images selected for our algorithm training did not contain homogeneous ice cover because the mixing of different ice types with different degrees of deformation, cracks, ridges and leads usually occur in ice covered areas.

**(17) page 6, lines 4-6:** please separate the single sub-classes more clearly. Is it 1: young ice, firstyear ice and multi-year ice, 2: fast ice, 3 broken ice mixed with ice-free water? What is the reason to group the ice types like that? Usually, e. g., young ice and multi-year ice reveal very different radar signatures (at least in intensity, not necessarily in GLCM textures). Younger ice can be misclassified as open water at lower wind speeds, multi-year ice as open water at higher wind speeds, if one focuses on radar brightness.

These subclasses were chosen empirically after several algorithm training attempts. We did not only define a number of texture features but also varied the combinations of subclasses. One subclass includes young ice, first-year ice and multiyear ice. The second is fast ice since backscatter and texture has similarity with calm open water. Young ice and multi-year ice can be misclassified as open water at lower or higher wind speeds, but the usage of texture features solved this problem in our case. The main problem was to detect correctly the transition zone from a general ice massif to ice-free area, where can close and very-close broken ice mix with ice-free water. And finally the sea ice class was subdivided into 3 subclasses. In other words, this approach is suitable in the case of obtaining only ice \ water separation.

**(18) page 6 line 14:** "the full range" refers to the number of grey tones, which are rescaled to a lower number of bits? How many bits do your original images have?

Originally the RS2 image has 16 bit unsigned integer type and the calibration in Nansat produces sigma0 values in 32 bits floating point format.

**(19) page 7, lines 5-8:** this is another very important part of your work which needs to be described a little more in detail. **(a)** You vary the computational parameters: window sizes, cooccurrence distances, and quantized grey levels (please mention the increments for the latter two). With these different computational parameters you calculate the different texture features – which means that you have a huge number of possibilities. By which method did you determine the optimal combination of computational parameters (which you mention on page 8 lines 25-30)? Is it described in your TGRS paper from 2013, to which you refer to in section 4.2? The TGRS paper, however, does not cover all aspects of the processing described here.

**(b)** Which criteria did you apply for deciding which combination of texture features is optimal for classification at HH- and at HV-polarization? (In your TGRS-paper you used all texture features.)

**(c)** How many radar images and related ice charts from Met. Norge did you use for these tests?

**(d)** Were the selected combinations of texture features best for all images, or only in a majority of the investigated cases?

**(a)** The list of experiments with values of the parameters is now added to the manuscript. The main approach to select the best combination turn out to be empirical testing on several images and qualitative assessment of the results at each step of the algorithm.

We clarified the text in Sections 3.4 and 4.2, and provided one more figure

(b) In TGRS-paper the correlation analysis and visual interpretation of normalized texture features distribution were applied. In this case we use the same technique.

(c) We used 24 training images noted in Sect. 2.

5 (d) The texture features combinations were the best for the majority of processed images.

(20) Section 3.6: For ice chart production, also optical images were employed. In how many cases could they not be used because of dense cloud cover? Did you use a “weight” indicating the reliability of the ice charts (assuming that the lack of optical information causes more difficulties for the ice analyst to separate ice and water)?

10 No, we did not use “weight” indicator - confidence level flag information.

(21) **Page 8, line 15:** what do you mean by “...and increases from top right to bottom left”? Do you refer to the extent of the open water area?

15 The sentence has been rewritten as follows: The open water area is located on the right-hand side of the image and the ice covered area - in the upper-left corner.

(22) **Page 8, lines 17-18:** Does new and thin ice really always appear brighter than OW at HV-polarization? I doubt this.

20 Not always, we mentioned the ice situation on this RS2 image. We agree with this remark and have corrected: The ice-covered areas and the rough OW areas appear both bright in HH and are therefore difficult to distinguish. Including HV, however, provides additional information, since OW areas on this image appear generally darker than sea ice in HV.

25 (23) **Section 4.1:** As already noted above (comment 15): How did you handle the computation of texture features in the zones along the borders between the image stripes that you indicated as white lines in 3b? When the sliding window reaches the first element of image stripes (masked by nan value) the all ‘masked’ stripe values are skipped, and the computation is continued when sliding window passes away the whole stripe’s “width”. Further the masked stripes are excluded from the result matrixes of texture features.

(24) **Section 4.2:** Please see comments (19). From my point of view it is up to you whether you provide more details about methodological aspects in section 3.4 or in this section 4.2. Please, see our answer for the comment 19.

35 The table that lists the experiments definitely belong to the methodology. The Results may refer to the number of experiment in the table.

(25) **Page 9, lines 3-5, Fig. 4:** The usefulness of the different texture features is not clear to me. When combining the intensities at HH and HV, calm OW is very well separated, but OW and ice partly overlap. The latter is also valid for the two graphs to the right, but here even calm OW overlaps with the ice. Please provide some convincing arguments why the texture features improve the water-ice separation? (See also comment 33 below).

The scatterplot of HH-pol energy vs. HV-pol correlation have been added.



Using only combination of HH and HV intensity, we can distinguish open water in some cases (Fig 1c below). The co-pol ratio was calculated, and then simple threshold was used to figure the OW area. Here OW was distinguished clearly with some artifacts on the other part of the image.

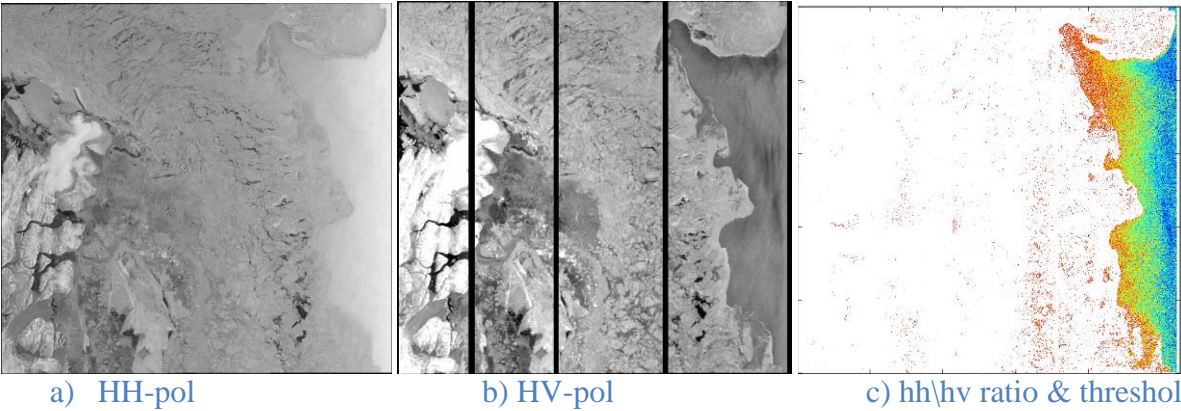


Figure 1.

But in the most cases it is insufficiently (Fig. 2c). If the only combination of the intensities at HH and HV will be applied in the classifier with preliminary training procedures, the result will not be satisfactory.

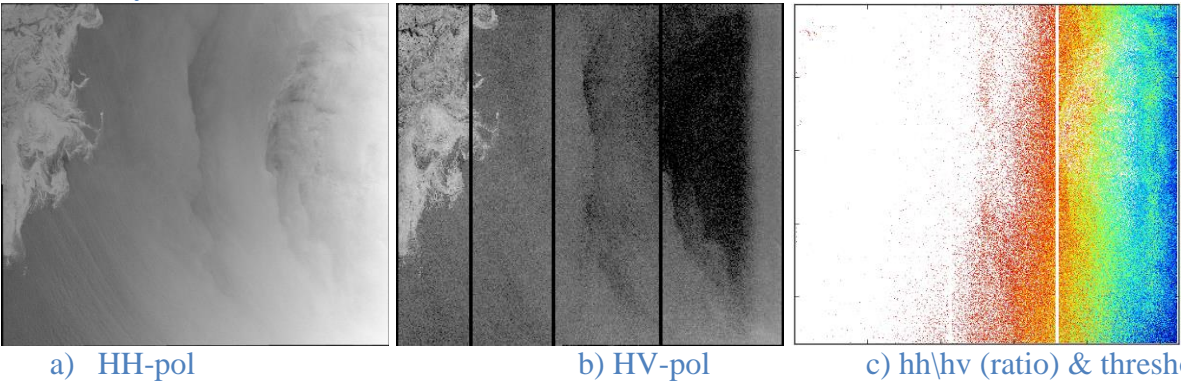


Figure 2.

We also provide some examples of other SVM, where all TF and only  $\sigma_{HH}$  and  $\sigma_{HV}$  were used for training process. Some statistics are provided. Please see our answer to comment 9 by Referee 2.

(26) Referring to Fig. 6, 7, 8: why is Fig. 5 not mentioned before them?

We have corrected this.

(27) Section 4.4: How was the comparison between classified radar image and Met. Norge ice charts carried out? Were the latter digitized to the pixel size of your radar images?

The comparison was carried out using pixel by pixel approach. The met.no ice charts were originally in digital form in stereographic projection. Our SAR-based classification results were subsampled and reprojected onto the coordinate system of the ice charts for further comparison.

5 (28) page 9 line 28-30: (a) “...ice charts WERE obtained manually...”; (b) what do you mean by “higher rate of thematic processing” in this context? I think that also ice charts from Met.Norway could include a higher level of details if the ice analyst delimits small-scale features. But this would require a longer time for ice chart production. What is the processing (computer) time needed when applying your algorithm compared to the semi-automated chart production by Met. Norge? This aspect is important and should be added to the discussion section 5.

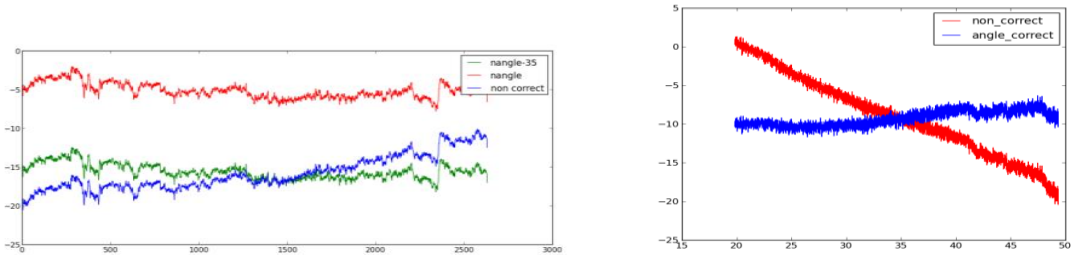
10 (a) We corrected this.

(b) We removed these sentences. Our developed automated algorithm allows computing a classification result in less than 15 minutes. Based on our experience with visual classification we can conclude that it may take up to several hours by an ice expert to produce the ice chart for users. Thus, our semiautomatic algorithm is much more efficient than the manual one.

(29) Section 5.1: (a) The title refers only to the incidence angle correction, but the noise correction is also dealt with, at least in the last sentence.

We have corrected the title as: Significance of incidence angle variations and thermal noise reduction.

20 (30) page 10, lines 5-6: “Strong dependence of the backscatter on incidence angle in open water surface... is significantly higher than for sea ice”. This statement is not true in any case, since the incidence angle sensitivity depends on the surface roughness: the smoother the surface, the larger the sensitivity (in particular close to the angle of specular reflection). Thin level ice can be very smooth and may show a larger sensitivity than a wind-roughened water surface.



a) Sea ice (coefficient = -0.29)

b) Open water rough (coefficient = -0.68 (- 0.76)

**Figure.** Angular correction of RS2 SAR image HH-channel along the whole swath a) sea ice b) open water).

The coefficients were obtained by the averaging of the derived angular dependencies of the backscatter for sea ice and open water rough from a series of RS2 SAR images in winter.

We also have the investigations for Envisat ASAR WS data. Angular dependencies of the backscatter for various sea ice types were derived from a series of Envisat ASAR WS images. They are shown in a Table below.



Table. Angular dependences of sigma0 for several sea ice types and rough open water with incidence angle increase for all images.

Ice type	Changes of sea ice backscatter with incidence angle increase, dB/degree
Water surface	(-0.82) – (-1.05)
Grey ice	(-0.14) – (-0.20)
First-year ice	(-0.18) – (-0.42)
Multiyear ice	(-0.16) – (-0.24)

5

**(31) (a) page 10, line 8:** what do you mean by “overestimated signatures”?

**(b)** Line 9: what do you mean by “ice cover has more reliable backscatter ranges for various ice types”? Since wind speed can be determined from radar measurements over open water, this means that also open water has clear defined ranges of backscattering intensity for a given wind speed and direction (except for OW patches within the ice cover and at the ice margin where ocean surface wave interactions are more complicated).

10

The sentences have been rewritten as follows:

Coefficients for angular dependence of water covered areas are significantly influenced by wind conditions - with stronger wind intensity grows faster. Our observations show that angular dependence of sea ice is more stable regardless of wind or other conditions. Since the surface type is not known a priori, we have to choose which angular correction to apply and the preference is given to the more reliable sea ice angular correction.

15

**(32) Section 5.2: (a)** You should make clear that in the first sentence you refer to the nine texture parameters given by equations 2-10. If you in addition use intensity and standard deviation, there are in total 22 parameters considering both HH and HV (and not 20). In the following text you should make clear that you now refer to section 4.2, in which you selected 5 textural parameters + intensity + standard deviation for HH, and 4 textural parameters + intensity for HV, leaving in total 12 parameters.

20

**(b)** I do not understand the meaning of the two sentences from line 20 to line 23. E.g., what are “poor features”? What is a discriminant function in this context, and why is it needed? If all features are used, does this mean that the classification accuracy is lower in any case? There is of course an optimal number and an optimal selection of textural features giving highest classification accuracy, but with, e. g., only 4 textural parameters you might theoretically still get better accuracies than with less parameters. The last 3 sentences of section 5.2 refer to the reduction of dimensionality but a direct link to the own processing described in section 4.2 is missing (e. g. the criteria for selecting some of the nine given textural features and excluding others).

25

30

**(a)** We agree that there is some confusion and corrected the text: one texture feature (cluster shade) was excluded from equations since actually we did not use it. Thus there are in total 20 parameters considering both HH and HV.

**(b)** ‘Poor features’ replaced by ‘informationally poor features’

**A** sentences have been modified and moved from section 5.2 to section 3.4 :

35

A selection procedure is applied to limit a set of texture characteristics that provides a good classification with a small computational load. This procedure includes visual assessment of scatterplots comparing values of texture features in different combinations. Candidate texture features that provide

the best separation of classes are selected and others are discarded. The selection procedure also uses a set of training image regions to establish the set of features and its computation parameters providing the smallest classification error. In other words, we constrain the texture features number by the demanded balance considering the SAR image level of details, computation time and the optimal reliable class separation.

**(33) Section 5.3:** With this section I had considerable difficulties. **(a)** I suggest that you provide a table giving the function of each textural parameter (e. g. measure of local variations), and the interpretation of the respective parameter related to Fig 5.

**(b)** In this section you introduce alternative denotations for the textural parameters (e. g. energy – angular second moment; homogeneity – inverse difference moment etc). You should make this clear by expressing it like “Energy (also called ‘Angular Second Moment’)...” (after this, it is fine to go on with e. g. “Homogeneity or Inverse Difference Moment”).

**(c)** page 10 line 30. I found that the “Energy” is the square root of the Angular Second Moment. Is

“repeatability” another denotation for energy? In Fig. 5i, the OW area, which appears homogenous in Fig. 3b, reveals a very low energy – is it a noise effect? The bright blue zones in the OW-area in Fig. 5i are due to the stripes in Fig 3b?

**(d)** page 11 sentence lines 6-7: I do not understand this sentence. The GLCM correlation function is calculated for a co-occurrence distance of 8 pixel? Fig. 5j: I do not understand why the correlation is very high in the marginal ice zone and low in the more closed ice. I would expect it vice versa. The low correlation value over open water is again a noise effect?

**(e)** page 11, line 13: homogeneity – why is the homogeneity high in the marginal ice zone and low in the inner ice zone and over water (Fig. 5k)? Again I expected this vice versa.

**(f)** page 11, line 17: “...indicates a random mixture of scattering mechanism”. I think here the entropy from the entropy-alpha decomposition described by Cloude et al. (where entropy is indeed related to the character of the scattering mechanism) is mixed with the GLCM entropy, which does not give any information about the scattering characteristics from within one pixel but relations between neighboring pixels.

**(g)** page 11, lines 26-28 and lines 30-33, regarding Fig. 4: I do not see a clear separation between OW (dark blue) and sea ice (green), and the separation capability of the texture features seems to be worse than the one of the intensities. See also comment 25 above.

The sub-sections 5.2 Number of texture features vs efficiency and 5.3 Meaning and value of texture features were merged and the text has been modified.

**(34) Section 5.4, first paragraph:** **(a)** it should be considered that the maps drawn by the ice analysts are a “smoothed version” of the ice cover variation. In principle the ice analysts could also provide more detailed maps. However, I anticipate that an automated algorithm can do this much faster – see also comment 28 above.

**(b)** why didn’t you use a better land mask?

**(c)** page 12 lines 17-20: how did you treat the beam boundaries when calculating the texture features (see also comment 23 above)?

**(d)** page 12, lines 32-33: why didn’t you exclude cases in which the temporal difference between manual and automatic ice chart was large?

- (a) Please, see our answer for the comment 28. We correct this.
- (b) In fact landmask has high resolution, 250 m indeed. In order to mask incorrectly classified subimages along the shore, where land pixels are mixing with water or ice pixels, the landmask was extended to also cover the sea. We remove this sentence.
- 5 (c) The all 'masked' residuals are skipped on the TF calculation step. Then it is excluded from the result images – this is a part of the algorithm. This lost information does not caused significant harm in the image scale.
- (d) We would like to test as much data as we can, and estimate the fully automated process – the SAR images were acquired and all of them were processed in the zone limited by the latitude and longitude values. Actually we just tried to make sense that the accuracy can have higher value, and the potential of this classification technique is high for the Sentinel-1a data processing.
- 10

## Reviewer 2:

### 15 1. P2L26- Dual-polarization has several

- C: The major advantage offered by the HH and HV polarizations is that they are results from different backscattering mechanisms.  $\sigma$  HH is dominated by first-order scattering (direct backscatter with no multiple reflections), whereas  $\sigma$  HV is a result of multiple scattering (two or more reflections involving two or more scatterers)). Hence it easy to understand that the magnitude of  $\sigma$  HV is usually smaller than the magnitude  $\sigma$  HH
- 20 . The energy radiated towards the radar decreases significantly with each reflection. Rewrite also the text in P4 L11-14 keeping in mind the above explanation and the comment (9) by Referee 1. E.g. increased ice deformation increases also the amount of the multiple scattering as does the large volume scattering component from MYI.
- We understand the mechanisms of HH\HV intensity difference. Here we mentioned the practical point of view of this advantage. Please, see our answer for the comment 9 by Referee 1.
- 25

2. P3L20-23. C: Here the authors could also comment why they have not targeted to produce a sea ice concentration chart which would provide to the users and modelers more information than a binary open water/sea ice chart. As we can see from Fig. 8 the presented classification chart (8d) is not a good
- 30 approximation for an ice concentration chart (8b).
- Ice types are required for many other users. Ice concentration is important but this parameter is calculated by other algorithms. This method aims estimate the several ice types. This paper is the first step to implement the algorithm where we distinguish the only ice \ water.

- 35 3. P4L5-8. C: Here you could add a remark that the classifier trained in the winter conditions is not ideal for the summer conditions.
- We have clarified this in text as: In summer the contrast between backscatter intensities of the melted different ice types observed on the SAR image is diminished since surfaces become smoother and is dominated by meltwater. The intensities are reduced as well as contrast between ice and OW.
- 40

4. P5 Sect. 3.1. and P8 Sect. 4.1. C: I strongly support the suggestion (14) of Referee 1. Otherwise the statistical incidence angle compensation that you use is left unclear. In Sect. 4.1 you give just number (0.298) without

units and with wrong sign. I assume that you mean the slope coefficient  $-0.298 \text{ dB/1}^\circ$ . I wonder why the magnitude of the coefficient is much larger than  $-0.196 \text{ dB/1}^\circ$  given in your 2013 paper for MYI or the coefficient  $-0.23 \text{ dB/1}^\circ$  estimated in Makynen et al. (2002) for FYI. It should be noted that in Makynen et al. (2002) the same targets in different images with different incidence angles are examined. If I have understood correctly, in your 2013 paper you have studied targets which looked similar but appeared in different incidence angle ranges in the same image. What kind of procedure have you followed here? Is the steeper slope due only to a different sensor or do some geophysical factors contribute, like sometimes less than 100 % ice concentration in the test images?

Please, see our answer for the comment 14. We derived angular dependences of backscatter for sea ice including different stages of development and deformation with a one degree step from calibrated RS2 SAR images at HH-polarization in winter period when the ice was observed continuously across the swath. There is no any geophysical factor since the images were taken from different parts of Arctic. We have corrected the slope coefficient according to the reviewer's remark.

**5. P6L2-7. C:** The referee 1 already commented this passage in the comments (16) and (17) which comments I support. My additional question is that what is the role of these subclasses in the classification scheme. Does SVM use them? If so, how have you selected all these subclasses as input to the classifier. Clarify the text please.

Please, see our answer for the comments 16, 17. The classification results were assessed using expert knowledge (please, see also comment 12 by Referee 1). We use these classes for training. The procedure of SVM learning in our case involves the following steps: 1) RS2 ScanSAR images for training were selected and pre-processed. 2) These pre-processed images were used for texture features calculations. 3) The expert analysis of RS2 ScanSAR images includes the identification of polygons with sea ice (3 ice types) and open water (calm and rough open water) delineation. These results were collocated with texture characteristics matrixes (obtained after step 2) to get a number of training vectors. Selected dataset was applied for SVM training as inputs. As result three ice types and types of different open water were taken.

We have clarified this in Section 3.3 as:

These manual classification results were collocated with texture feature images (description provided in Sect. 3.4 and 4.2) to get a number of training vectors. For the final product the subclasses were merged into the main classes 'sea ice' and 'open water' since the similarities between the subclasses are too high for a reliable discrimination without additional data.

**6. P7L5-8. C:** An addition to the comment (19) of the Referee 1. Yu et al. 2012 (in your reference list) have applied to the feature selection problem "a forward feature search" which is identical to the forward stepwise selection in the regression analysis. The only difference is that in the feature selection the criterion is the classification accuracy instead of the criteria like AIC, BIC and many others used in the selection of the variables in the regression model.

Please see our answers to the comment 19 by Referee 1.

We have estimated obtained SVM versions with different TF combinations by testing it on our special "test" list. This test list was formed after the several algorithm training attempts and includes the most difficult situations for automated classification like: the open water areas with different surface features

caused by wind and currents represented a significant problem, several difficult situations in “transition zone” - area between a general ice massif and ice-free area, etc. The SAR images of the test list partly belong to the training list.

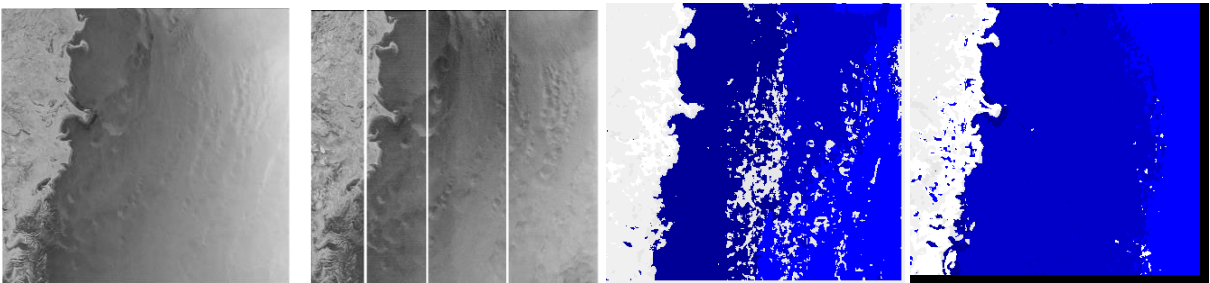
- 5 **7. P7:** Section 3.5. The description of the SVM is given in a very general level and the text is not well organized. The presentation should be more informative. You have many alternatives to detail your presentation. One is that you formulate the SVM as a solution to an optimization problem (e.g. Hastie et al, The Elements of Statistical Learning, available as a PDF file in the internet) and comment its properties from this point of view. Another approach is to treat the problem as Yu et al. 2012 (mentioned above) have done. In any case you must estimate some parameters when fitting the SVM in your data. Give the estimation method. When someone reads your text, he/she should get an idea what the SVM is and why you have chosen it. The equations are in this context necessary. The SVM gives only a binary classification result. Explain how you have generalized it into the case of three classes (like in Fig. 8c).
- 10 We have specified and corrected description of the SVM in the paper. We have not included the equations of the decision function and RBF kernel, since there are well-known and can be found in any SVM book or paper. The references are provided.
- 15

**8. P8L11.** C: Is the radar look direction in Fig. from right to left?

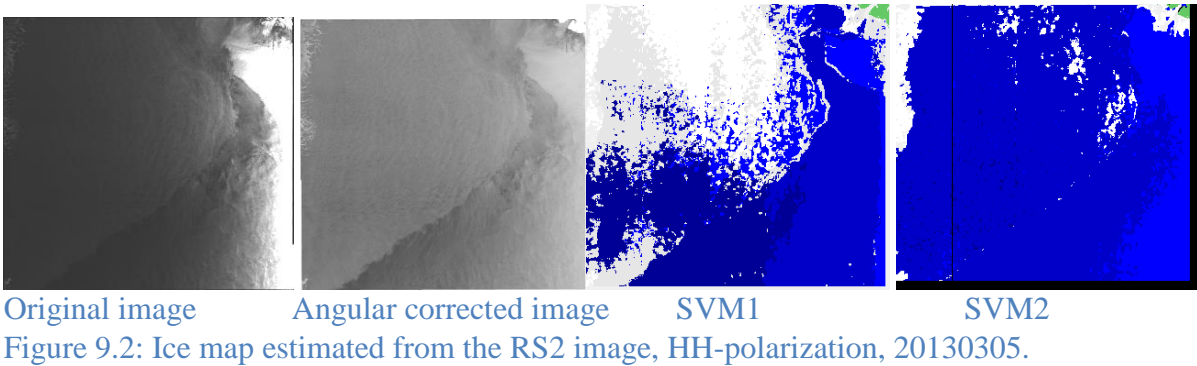
- 9. P9L3-5.** C: I agree with Referee 1 (comment (25)) that Fig. 4 shows no increased discrimination ( $\sigma_{HH}$ ,  $\sigma_{HV}$ ) pair. When looking at Fig. 5 my ability with the texture features when compared to the subjective opinion is that Figs. 5a and 5h (corresponding to the HH and HV channels) provide the two best features. Show how the classification accuracy improves when you add texture features to the ( $\sigma_{HH}$ ,  $\sigma_{HV}$ ) pair. The sentence in P9L1-2 is not an argument.
- 20 We agree with this remark, and corrected the sentence: Texture characteristics provide a more complete delineation of surface parameters in addition to the raw backscatter signal, and increase the potential for ice and water separation.
- 25 The new scatterplot was added.

Please see our answer to comment (25) by Referee 1.

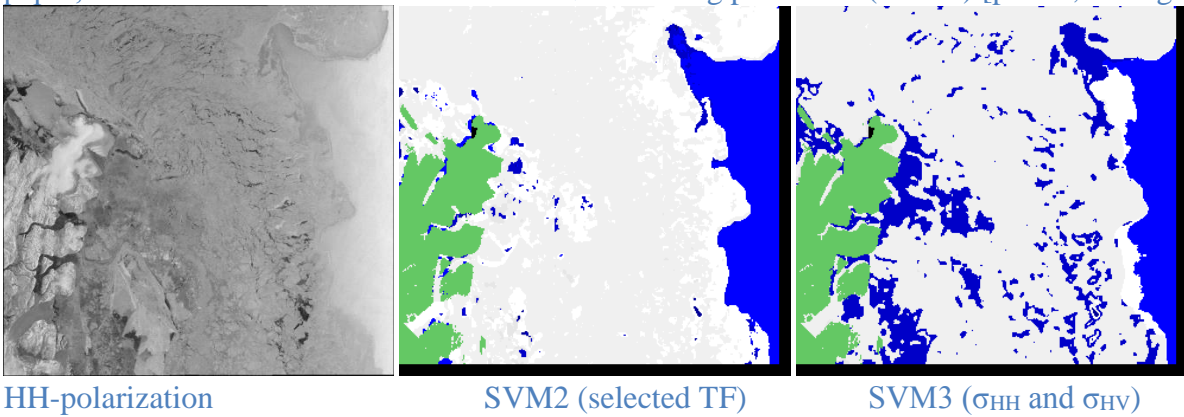
- 30 We produce several versions of SVM. The figures below present the classification results of SVM, when the whole set of TF were used for training (SVM1). Training of SVM2 was based on our selected TF (working version used for automated classification).



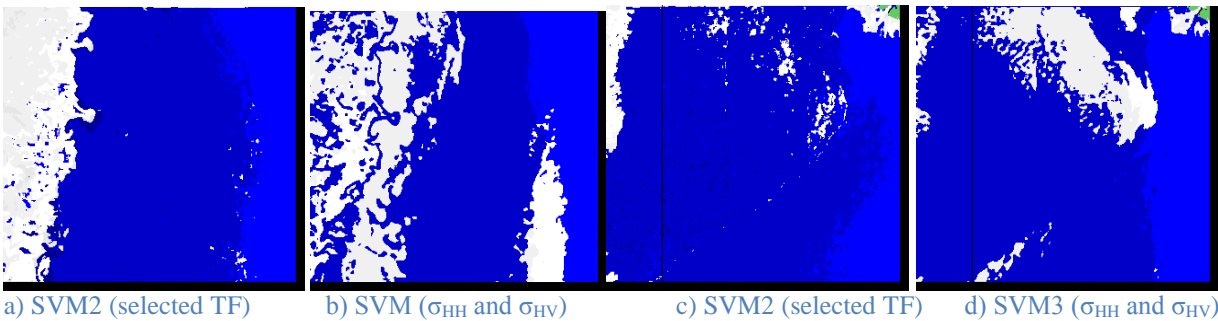
35 HH-polarization HV-polarization SVM1 SVM2  
Figure 9.1: Ice edge map estimated from the RS2 image, 20130318.



- 5 To present the usefulness of TF, we have trained few SVM with only 2 input parameters -  $\sigma_{HH}$  and  $\sigma_{HV}$ . Several SAR images were classified by SVM (SVM2) using in our automated algorithm presented in paper, and version of SVM with  $\sigma_{HH}$  and  $\sigma_{HV}$  in training procedure (SVM3) [please, see figures below].



- 10 Figure 9.3: Ice map estimated from the image, HH-polarization, 20111122. Blue – open water, grey \ white – sea ice, green – land mask.



- 15 Figure 9.4: Ice map estimated from the image, a, b) 20130318; c, d) 20130305. Blue – open water, grey \ white – sea ice, green – land mask.

The estimation of several RS2 images (accuracy, ice and ow errors) classified using SVM1, SVM2 and SVM3 are presented in Table below. The error matrixes based on pixel-by-pixel difference between



algorithm results and METno charts have been calculated for each RS2 image (listed in Table). Overall accuracies of OW and sea ice correspondence (Ov acc) and the impact of each class to the classification error (errors in ice and water classification – ow err, ice err, respectively) were computed.

	RS2 image	SVM1 (all TF selected)			SVM2 (TF selected)			SVM3 ( $\sigma_{HH}$ and $\sigma_{HV}$ )		
		Oc acc	ow err	ice err	Oc acc	ow err	ice err	Oc acc	ow err	ice err
1	RS2_20130206_	96.500	0.044	3.456	95.700	0.044	4.256	75.322	0.030	24.647
2	RS2_20130206_	96.409	0.000	3.291	94.309	0.000	5.691	61.043	0.000	38.957
3	RS2_20130207_	95.6	0.58	3.784	95.889	0.327	3.784	69.442	1.337	29.221
4	RS2_20130227_	95.889	0.327	3.784	93.045	0.626	6.329	56.986	0.159	42.856
5	RS2_OK37130_	95.586	0.017	4.614	94.068	0.008	5.924	64.905	0.018	35.077
6	RS2_20130313_	80.913	17.86	0.411	95.450	0.893	3.657	29.607	8.101	62.291
7	RS2_20130314_	88.340	9.236	2.424	91.996	0.138	7.866	43.742	5.999	50.259
8	RS2_20130401_	85.428	12.57	1.998	88.691	0.371	10.937	32.271	4.294	63.435
9	RS2_20130403_	93.142	3.860	2.998	93.239	0.446	6.314	26.798	6.862	66.340
10	RS2_20130416_	84.024	15.199	0.778	94.544	1.459	3.997	37.667	8.474	53.859
11	RS2_20130420_	69.692	27.336	1.516	93.031	2.183	4.786	26.037	8.710	65.253
12	RS2_20130425_	87.011	12.441	0.548	94.251	0.246	5.504	45.462	8.027	46.511
13	RS2_20130430_	59.403	37.231	3.366	93.658	0.443	5.899	29.038	28.24	42.720
	wind stripes & eddies [current]									
14	RS2_20130301_	85.135	12.327	2.538	91.411	3.429	5.160	41.724	1.547	56.729
15	RS2_20130301_	84.097	15.175	0.729	97.444	0.725	1.831	66.186	9.863	23.950
16	RS2_20130304_	72.827	27.114	0.059	97.002	1.609	1.389	53.131	0.112	46.757
17	RS2_20130305_	42.675	55.731	1.593	83.854	9.518	6.627	36.714	4.656	58.630
18	RS2_20130305_	58.442	41.558	0.000	96.925	2.300	0.775	58.391	0.471	41.138
19	RS2_20130306_	84.726	14.309	0.965	93.524	0.269	6.207	26.812	0.310	72.878
20	RS2_20130319_	57.011	42.989	0.000	85.124	14.43	0.446	53.895	17.88	28.221
21	RS2_20130408_	92.325	5.291	2.384	92.159	0.496	7.345	14.425	3.379	82.195
22	RS2_20130408_	85.609	13.881	0.510	92.899	2.030	5.071	15.574	0.702	83.723

- 5
- Correct detection of open water areas with different surface features caused by wind and currents represented a significant problem for automated classification that motivated us in our research of TF selection. Visual analysis (Fig. 9.1 – 9.2) and inspection of overall accuracies of SVM1 and SVM2 shows that although the sea ice delineation is more accurate (images 1-13 in Table), the optimal TF number can improve OW detection (the images from 14 to 23 in Table contain different the most difficult features for automate detection on the OW surface).
- 10
10. P9L2. ... methodology description... C: What did you mean by this? In the 2013 paper you selected all the features. Please clarify.

15 Please, see our answer for the comment 19 by Referee 1.
11. Sect. 4.2. and Fig.4. C: How have you normalized the features? As Fig. 4 shows the ranges of different textural features are highly variable. It would also be better if the normalized values of the textures (as in Fig. 5) would be used in Fig. 4. In any case the SVM requires that normalized feature values are used or the distance concept in the radial basis function is arbitrary.

20 All features were normalized for SVM training \ application using defined mean and standard deviation values of each TF from all training images. The subimages of figure 4 were corrected.

**12. Fig. 8.** In the figure caption: ...open water (ice concentration from 0 to 15%)... C: How have you identified such areas? The manual ice charts has the ice concentration classes: 0/10 -1/10, 1/10 -4/10 and so on. The class 0/10 -1.5/10 is missing.

In our previous calculations we used ice concentration data from OSI-SAF database, where the 15 % threshold was used for OW and ice separation. In this case for validation of automated classification result we use ice charts from METno with threshold amounts 0/10.

We agree with this remark and corrected this.

**13. P9L28-30.** C: I disagree with your conclusion that the SVM classification gives a more detailed ice cover map than the manual ice chart. If we inspect Fig. 8b we see how the sea area is divided into subareas with different ice concentrations. In Fig. 8e you have thrown away all this valuable information and forced the manual ice chart to a binary map. The comparison between the automated and manual chart that you have presented in the text is not fair. Please modify your text and assessment.

We understand that all ice services (not only met.no) in their manual interpretation can produce very detailed high quality ice charts with rather high accuracy of the ice situation. And in any case we were not going to dispute the valuable and accuracy of met.no charts since we use it as the best available information for validation. The text was modified.

**14. Sect. 5.2.** C: An addition to the comment (32) by the Referee 1. Do you have considered the principal components as a way to deal with the intercorrelation of the features and simultaneously reduce the dimensionality? If you have, why did you reject the principal component analysis.

We have tried this approach in our previous attempts of RS2 classification using Neural Networks. The PCA was applied to reduce the TF number in input vector. The visual analysis of classification results and the estimated accuracies were not so satisfactory.

**15. Sect. 5.3.** C: As the Referee 1 (the comment (33)) I struggled and often failed to understand your interpretations of the texture measures. This section had to be rewritten, e.g. following the guidelines given by the Referee 1. Just one addition. As far as I know, the only scattering mechanism one is able to measure from the dual-polarized HH +HV image is the depolarization ratio. In the decibel .scale the depolarization ratio is simply the difference  $\sigma_{HV} - \sigma_{HH}$

Also please see our answer to the comment 25 by Referee 1.

**16. P12L4-5.** C: I disagree with you due to the same reason as earlier. I think that for the models a sea ice concentration estimate at coarser resolution is a better option than knowledge of locations of small open water patches or leads.

Also please see our answer to comment 2 and 9.

**17. P12L6-8.** C: It is possible to derive a land mask from the MODIS data at resolution of 250 m. So the difference is not big compared to RS2 data, especially when we take into account that the resolution of the final product is 1.6 km (P5L6). Why do a MODIS based land mask underestimate the land area? I would expect that it might slightly overestimate it.

In fact landmask has high resolution, 250 indeed. In order to mask incorrectly classified subimages along the shore, where land pixels are mixing with water or ice pixels, the landmask was extended to also cover the sea.

- 5 18. P12L15. ...different structures on the water affected by wind and .. C: Eddies are not caused by winds. They are results of ocean currents. Write ...affected by wind and currents ..

Yes, of cause eddies are results of ocean currents. We agree with this remark and have corrected the text.

10 **Reviewer 3:**

**General Comments:** 1. Too often are new image classification algorithms just assessed on a few test images and as a result are not very robust. A strength of this paper is that the algorithm the authors present is tested over a great number of images. In this regard, the classification results are very good over the annual cycle and while their Table nicely summarizes this result it would be useful to showcase the classification results in more detail. Specifically, I think readers would like to actually see (visually) the performance of this algorithm during the summer melt or more difficult classifications – I know, I did after reading this paper. I suggest adding a few more examples or even a panel figure of classification comparisons with ice charts highlighting algorithm performance visually. They do not have to be perfect but for operations that does not matter – ice analysts want to see how the algorithm will perform in the most difficult conditions.

- 20 Please see the figures for the comment 9 by Referee 2.

Yes, it is possible to add more examples, but we don't want to extend the number of figures and would like to maintain the existing layout of the paper.

**2. The English structure requires some serious attention. There are numerous passages that are difficult to follow or just do not make sense. I suggest a thorough English edit be required before publication.**

- 25 **3. The manuscript structure can be improved by combining the results (Section 4) and discussion (Section 5) sections. As it reads now, certain sub-sections of the discussion do not reference material created in the analysis which they should do (i.e. 5.1, 5.2). For example, the discussion on incidence angle has no reference to the correction the authors applied. Validation and Sources of Error can be easily compared and would make for a better read.**

- 30 **4. Perhaps more important than 2 and 3, it is not clear from the text (4.2/5.2) how the optimal texture combinations where chosen? I think this needs to be addressed in the methodology not the results. Nevertheless, this a remains a major problem that needs to be clarified.**

Please, see our answer for the comment 19 by Referee 1.

- 35 **Overall, I think the algorithm presented in this paper is worthy of publication when the comments outlined above and below are taken into consideration.**

**P11L22: I don't think exploring is the correct word. Perhaps quantifying?**

We rewrote the sentence.

40

**P11L24: regions not region**

We have corrected this sentence.

- P1L25: such as ERS-1/2  
We have corrected this sentence.
- 5 P1:30: that extend operational utility.  
We have corrected this sentence.
- 10 P2L1: The objective of sea ice classification is to identify sea types and open water. You do not need “based on” unless you are going to mention everything taken into consideration.  
We have corrected this sentence.
- 15 P2L5: That is basically all factors. Why not just say discriminating between open water that is wind roughened and sea ice is difficult?  
We have corrected this sentence.
- 20 P3L4: The CIS did not developed MAGIC. To my knowledge it was developed by Dr. Clausi at the University of Waterloo.  
Yes, the MAGIC (or MAGSIC) was developed in University of Waterloo by the MAGIC research group (Clausi, Maillard, Deng etc). MAGSIC had shown promising results and is being encouraged by CIS. Now MAGSIC is a modular system being developed as an operational tool to be inserted into CIS operations. We agree with this remark and corrected the text.
- 25 P3L20: The goal is not to extend ENVISAT single polarization, it is simply to utilize dual polarization data for ice classification.  
We agree with this remark and corrected this sentence.
- 30 P3L30: ice conditions.  
This section contains some technical details of utilized SAR data and the study area as well as ice conditions on the winter images are described. So we think that “DATA” is more common title for this section.
- 35 P4L10-20: No need to describe what HV is. Start with: The HV channel...but this is a difficult passage to follow on the physics as to why HV is darker than HH in RADARSAT-2. I suspect English is the root cause. Revise.  
Please, see our answer for the comment 9, 10 by Referee 1.
- 40 P4L22-33: It would be better if the methodology was written out in paragraph form rather than numbered points. You can still include numbers (i.e. i, ii, iii, etc) in the text.  
We have decided to keep this style.
- P5L13: Why not just simply state that the imagery was normalized to 35 degrees and move on? IA correction does not require a separate sub-heading.  
We followed to the comment 14 by Referee 1. Also please see our answer to the comment 4 by Referee 2.

P5L30: Unclear what is meant by Manual classification has be done. . .? Did the author's manually classify the imagery? It is unclear what is trying to be communicate in this sub-heading.

[We have clarified this section.](#)

- 5 P6L10: Are all the texture features used in the classification or just some? How are certain ones selected over others? This needs to be clear in the text. See General Comment 4.

[Please, see our answer for the comment 19 by Referee 1.](#)

- 10 P8L5: Is there a website link to the MET ice charts? Do they use RADARSAT-2 imagery? If they do not, this should be mentioned as they are an independent source for comparison.

[We have added a website link to MET ice charts. We mentioned in text that they use also high resolution SAR images \(RS2 and Sentinel-1A\) in the analysis.](#)

P8:10: Why is figure 6 being introduced before the other figures?

- 15 [We have corrected this.](#)

P13L6: developed, not proposed.

[But we already developed the algorithm and now proposed the algorithm description in this paper.](#)

- 20 Figure 2: Needs some latitude/longitude information for reference

[Done.](#)

Figure 3: Needs geography similar to Figure 2. The line graphs need to include axis labels and the font needs to be bigger.

[Done.](#)

- 25 Figure 6. Labels a) and b) are not included on the image

[Done.](#)

# Operational algorithm for ice/water classification on dual-polarized RADARSAT-2 images

Natalia Zakhvatkina<sup>1,2</sup>, Anton Korosov<sup>3</sup>, Stefan Muckenhuber<sup>3</sup>, Stein Sandven<sup>3</sup>, Mohamed Babiker<sup>3</sup>

<sup>1</sup>Nansen International Environmental and Remote Sensing Centre (Nansen Centre, NIERSC), 14th Line 7, Office 49, Vasilievsky Island, St. Petersburg, 199034, Russian Federation

<sup>2</sup>Arctic and Antarctic Research Institute (AARI), Bering str. 38, St. Petersburg, 199397, Russian Federation

<sup>3</sup>Nansen Environmental and Remote Sensing Center (NERSC), Thormøhlensgate 47, 5006 Bergen, Norway

*Correspondence to:* Natalia Zakhvatkina (natalia.piotrovskaya@niersc.spb.ru)

**Abstract.** Synthetic Aperture Radar (SAR) data from RADARSAT-2 (RS2) in dual-polarization mode provide additional information for discriminating sea ice and open water compared to single-polarization data. We have developed an automatic algorithm based on dual-polarized RS2 SAR images to distinguish open water (rough / calm) and sea ice. Several technical issues inherent in RS2 data were solved in the pre-processing stage including thermal noise reduction in HV-polarization and correction of angular backscatter dependency in HH-polarization. Texture features were explored and used in addition to supervised image classification based on Support Vector Machines (SVM) approach. The study was conducted in the ice-covered area between Greenland and Franz Josef Land. The algorithm has been trained using 24 RS2 scenes acquired in winter months in 2011 and 2012, and the results were validated against manually derived ice chart product of the Norwegian Meteorological Institute. The algorithm was applied on a total of 2705 RS2 scenes obtained from 2013 to 2015, and the validation results showed that the average classification accuracy was  $91 \pm 4$  %. The next step will be to adapt and apply the algorithm for classification of several ice types using Sentinel-1A/B as the main data source.

## 1 Introduction

Synthetic Aperture Radar (SAR) is an active microwave sensor providing high resolution images over large areas independent of clouds and daylight. This is especially useful for observing the polar regions where SAR data are widely used for exploring sea ice concentration, extent, detection of leads, polynyas, ice floes and ice edge, ice type identification and classification (Johannessen et al., 2007; Dierking, 2013). Monitoring of sea ice process, i.e. ice edge variations and motion, is important for practical tasks such as ice navigation and for scientific studies. High-resolution data from C-band SAR such as ERS-1/2 (European Remote Sensing satellites, European Space Agency (ESA)), RADARSAT-1 (Earth observation satellite, Canadian Space Agency) and ENVISAT (Environmental Satellite, ESA) have been used as the main data source for sea ice monitoring in the last two decades (e.g. Johannessen et al., 2007). The advanced capabilities of SAR on board of RADARSAT-2 (RS2) and Sentinel-1 (European Commission and ESA) with multi-polarization data can improve sea ice observations such as ice edge detection and ice type classification.



SAR images can be used to identify different sea ice types and open water (OW) areas based on variations of the backscattered radar intensity (caused by surface roughness) and other sea ice properties. Classification methods based only on the backscattering coefficients ( $\sigma^0$  or  $\sigma^\circ$ ) are hampered by ambiguities in the relation between ice types and  $\sigma^\circ$ , since various ice types (multiyear, first-year and some young and new ice) and open water depending on wind speed and direction can have similar  $\sigma^\circ$  (Dierking, 2010; Johannessen et al., 2007). In particular discrimination between low wind open water (calm open water) and first-year ice, young ice with frost flowers and multiyear ice can be problematic. Including additional image characteristics like image texture, tone, spatial structures, can improve the classification results significantly (Shokr, 1991; Soh and Tsatsoulis, 1999; Clausi, 2002; Bogdanov et al., 2005; Maillard et al., 2005; Yu et al., 2012).

Numerous efforts have been made to develop algorithms to retrieve sea ice variables from SAR data. The SAR polynya detection algorithm proposed by Dokken et al. (2002) is based on wavelet transforms for edge detection and standard texture-based methods. To classify sea ice and water for polynya detection, a threshold function using texture information is used. A semi-automated sea ice classification method based on fuzzy rules was reported by Gill (2003) for classification of RADARSAT-1 data over the Arctic into calm water, wind-roughened water, and sea ice in low and high concentrations. Advanced Reasoning using Knowledge for Typing of Sea Ice (ARKTOS) (Soh et al., 2004) has been established to support scientific research and operational applications in the field of sea ice segmentation and classification. Haarpainter and Solbø, (2007) developed an automatic algorithm for ice/ocean discrimination in RADARSAT-1 and ENVISAT SAR imagery. The texture based algorithm consists of an automatically trained maximum likelihood classifier and divides the SAR images into slices of small incidence angle range. The results show that sea ice and water can be discriminated quite reliably. Some examples showed a tendency of the algorithm to a better performance at low incidence angles. Karvonen et al. (2005) distinguished the Baltic Sea ice from open water on SAR images based on thresholding of segment-wise local autocorrelation. The method provided 90 % accuracy compared to digital ice charts for the Baltic Sea. This algorithm has been used by the Finnish Meteorological Institute (FMI). Tests with RADARSAT-2 and ENVISAT SAR data show that over 89.4 % of the test data fits the ice classification provided by the Finnish Ice Service for the Baltic Sea and Arctic Sea (Karvonen, 2010, 2012).

Dual-polarization has several advantages for sea ice classification compared to single-polarization SAR data. Young ice and multiyear ice, while being very different in their thickness (10 – 15 cm and more than 2.5 m, respectively), show rather similar brightness in the HH channel whereas MYI is brighter than young ice in the HV channel. First-year ice (level) is darker in both HH and HV and can be easily distinguished with young ice and MYI. Young ice and the wind roughened open water can both be difficult to distinguish from the sea ice in a single HH polarization. However open water especially affected by wind is darker in HV that improves sea ice classification (Sandven et al., 2008). The dual-polarization ENVISAT SAR Alternative Polarization Mode data enabled discrimination of sea ice types and open water with decision-tree classifier using estimated statistical thresholds for winter. Open water can be unambiguously discriminated (except thin sea ice) from smooth FYI, rough FYI, and MYI with > 99% accuracy using a co-polarized ratio threshold (Geldsetzer and Yackel, 2009).

The possibilities of supervised K-means and maximum likelihood classification of various SAR polarimetric data to three pre-identified sea ice types and wind-roughened open water was explored in Gill and Yackel (2012).

A MAP-Guided Sea Ice Classification System (MAGIC) for automated ice-water discrimination on dual polarization images from RADARSAT-2 combines a “glocal” Iterative Region Growing using Semantics (IRGS) classification (Yu and Clausi, 2008) with a pixel-based Support Vector Machine (SVM) approach. The “glocal” classification identifies homogeneous regions with arbitrary class labels. The ice-water map created with the SVM classifier exploiting SAR texture and backscatter features. The MAGIC system has been applied on 20 RS2 scenes over the Beaufort Sea. The average classification accuracy with respect to manually drawn ice charts is 96.5% (Clausi et al., 2010; Ochilov and Clausi, 2012; Leigh et al., 2014).

A Neural network (NN) based algorithm has been developed for ENVISAT SAR images for operational sea ice classification including validation (Zakhvatkina et al., 2013). The algorithm discriminated level FYI, deformed FYI, MYI and open water/nilas in the high Arctic in winter conditions and demonstrated good applicability in the Central Arctic. Using the same approach an algorithm for mapping ice / water utilizing ENVISAT ASAR WSM images was created for automated ice edge detection in Fram Strait. The ice / water classes were estimated by a multi-layer perceptron (MLP) neural network which uses SAR calculated texture features and concentration data from AMSR (Advanced Microwave Scanning Radiometer) and, later, SSM/I (Special Sensor Microwave/Imager) as inputs (Sandven et al., 2012). Daily ice/water products were provided with a resolution of 525 m from winter 2011 until April 2012. The accuracy of this classification was about 97 % compared to high resolution sea ice concentration charts based on manual interpretation of satellite data provided by the Norwegian Meteorological Institute.

Our goal is to extend the method originally used for the single polarized ENVISAT SAR images (Sandven et al., 2012) by utilizing dual polarization data from RS2 and to develop an algorithm for ice/water classification which can be applied to RS2 data for the production of ice/water maps as part of marine services under the Copernicus programme. A special motivation for our work was not only development of an algorithm but also its extensively validation in various sea ice conditions and identification of the applicability conditions. We also aimed at realization of the algorithm as an open source software available for other scientists. Our algorithm is based on texture features and SVM method using the advantages of dual-polarization RS2 SAR image data.

The paper describes the developed algorithm and discusses practical issues of its applicability. The steps and parameters for implementation of the algorithm are described allowing users to test the algorithms themselves. The paper is organized as follows: Section 2 introduces the satellite images and geographical area used in the study. The algorithm including pre-processing and validation procedure is described in Section 3. Results of the pre-processing step, ice/water classification and comparison with manual ice charts are given in Section 4. Finally, discussion of the results is presented in Section 5.

## 2 Data

The region of interest is the ice-covered sea between Greenland and Franz Josef Land where detailed ice information from SAR data is important due to the highly variable sea ice conditions, in particular the export out of the Arctic through Fram Strait (Vinje and Finnekåsa, 1986). SAR is the most useful sensor to provide high-resolution year-round data for estimation of sea ice variables such as ice classification, ice edge variability and ice drift.

This study is based on RS2 ScanSAR Wide (SCW) mode images with 500 km swath width, a pixel spacing of  $50 \times 50$  m and dual-polarization (HH+HV). This is the main mode used by RS2 for operational sea ice monitoring (RS2 Product Description, 2011). Twenty four SCW scenes around Svalbard (Fig. 1) of 2011 and 2012 were utilized in the following analysis to train the algorithm. The winter-month images were selected to cover various types of thin ice (e.g. new and young ice), first-year and multiyear ice with different degrees of deformation, packed ice, broken ice and open water under different wind speed conditions (rough, very rough and calm water including leads and dark nilas). The radar images include the most typical samples since the radar intensity contrast between open water and ice varies greatly with ice conditions and wind speed/direction which significantly affect the radar brightness of open water. In summer the contrast between backscatter intensities of the melted different ice types observed on the SAR image is diminished since surfaces become smoother and is dominated by meltwater. The intensities are reduced as well as contrast between ice and OW.

The backscatter at HH generally decreases with increasing incidence angle (Fig.2a), whereas the HV channel is less sensitive to the incidence angle. The HV channel includes disturbances in azimuth direction (visible as bright and dark stripes) along the burst boundaries in the ScanSAR Wide Beam SAR image (Fig. 2b). The expected noise level is a local mean noise power value that fluctuates across the image. The noise level is obtained from a model that accounts for the characteristics of the payload, the beam mode, the acquisition, and the ground processing [RS2 PUG] (Jefferies, 2012). The system noise level as a function of the incidence angle is documented in the XML file that comes with the RS2 image.

## 3 Methodology

Our semiautomatic ice / water classification algorithm comprises six main steps:

- 1) SAR data pre-processing including reduction of thermal noise effect for HV, incidence angular correction for HH, and absolute RS2 image calibration to obtain  $\sigma^\circ$  values for both channels.
- 2) Manual classification of SAR images into predefined classes (e.g. open water and ice of various types depending on which classes are needed). The predefined classes take into account information from optical data, ice concentration from passive microwave, previous classification results and historical data.
- 3) Calculation of texture features from HH and HV images.
- 4) Training of classifier (e.g. SVM) for classification of arrays with certain texture features as well as  $\sigma^\circ$  values based on the results of manual classification.
- 5) Application of automatic classifier to divide the RS2 scene into the predefined classes.

6) Validation of the classification results using manually drawn ice charts.

After completing the algorithm training, the fully automated image classification includes only three of the above mentioned steps: 1) reprocessing; 3) texture feature retrieval; and 5) application of the automatic classifier (SVM).

The initial size of the full resolution RS2 SCW image is about  $10000 \times 10000$  pixels. We downscale the original image by averaging to  $5000 \times 5000$  pixels to increase the computational efficiency and decrease the influence of speckle noise. The image size is further reduced during the computation of the texture features by using a sliding window with 16 pixels step size (the detailed parameters are described in Sec. 4.2). The image size of the final product is about  $330 \times 330$  pixels with 1600 m pixel spacing. This reduction in resolution significantly increases the processing speed and allows computing a classification results in less than 15 minutes.

- 10 Pre-processing of RS2 data was performed utilizing the open source Python toolbox NANSAT (Korosov et al., 2015), [https://github.com/nansencenter/nansat/wiki]. The texture extraction algorithm was created in the Python programming language. The scikit-learn open source was used to implement the SVM classification method [http://scikit-learn.org/stable/index.html].

### 3.1 Incidence angle correction for HH

- 15 The auxiliary XML files coming with the product, i.e. scaling Look-up Table (LUT), provide information for georeferencing and calibration. These LUTs allow converting the processed digital numbers of the output SAR image to calibrated values. An important goal of radiometric calibration is to provide the proper comparison between the scattering of image targets with different SAR sensors or from the same sensor with different operating conditions, so the backscatter values of targets can be compared to one another or a reference. Absolute radiation calibration is used to convert the digital numbers in the
- 20 SAR image to  $\sigma^\circ$ , applying a constant offset and range dependent gains to the SAR image (RS2 Product Description, 2011):

$$\sigma_j^\circ = 10 * \log_{10} \left( \frac{(DigitalNumber_j^2)}{A_j} * \sin(\theta_j) \right) - (coefficient * (\theta_j - 35))$$

where:  $\sigma^\circ$  - backscatter values in  $j$ -th range direction pixel in dB, *Digital Number* - pixel brightness (data consist of the SAR amplitude value *Amp* and intensity value  $I = Amp^2$ ), *A* - gain value (invariant in line) corresponding to the range sample  $j$  (obtained by linear interpolation of the LUT supplied gain values),  $\theta$  - incidence angle for each  $j$ -th pixel, *coefficient* - predefined calculated coefficient.

- All images are corrected to a reference angle of  $35^\circ$ , which represents the centre incidence angle and allows analysis of the SAR images without brightness amplification. Backscatter recalculation to  $35^\circ$  incidence angle is carried out using a predefined calculated coefficient. The coefficient was defined by calculating the linear trend of the observed backscatter signal on several HH-polarized RS2 SCWA images of pack ice. The procedure is similar to the pre-processing of ENVISAT
- 30 ASAR data in Zakhvatkina et al. (2013). The backscatter normalization to a pre-defined incidence angle provides

homogenous image contrast across the swath over ice-covered areas. The details of the angular correction method specificity are discussed in Sect. 5.1.

### 3.2 Thermal noise correction for HV

5 The thermal noise reduction consists of three steps: 1) reading 100 noise values and corresponding incidence angles from the XML file; 2) interpolation of noise on a finer grid for each pixel; 3) subtraction of interpolated noise values from the backscatter values of the entire image.

Due to the discontinuity of the noise floor at the boundaries of the individual SAR beams and the low resolution of the provided noise values in the XML file (only 100 points for 500 km swath width), the noise correction may result in an erroneous subtraction of a high noise floor from a low signal of the neighbouring SAR beam and hence, yield negative values for  $\sigma^\circ$ . To prevent such flaws, a 10 pixels wide stripe of data along the edge of the SAR beam is masked out and disabled for further analysis.

### 3.3 Manual classification

Manual classification has been done for the training images containing several different sea ice types and ice-free areas with both rough and smooth open water. Predominant subclasses which must be reliable and undertaken with good quality were identified and chosen by sea ice experts through visual analysis of RS2 scenes based on their previous experience. The images selected for our algorithm training did not contain homogeneous ice cover because the mixing of different ice types with different degrees of deformation, cracks, ridges and leads usually occur in ice covered areas. The main class 'sea ice' was chosen to include the following subclasses: 1) subclass including young ice, first-year ice and multiyear ice; 2) fast ice; and 3) broken ice on the edge (border) mixed with ice-free areas (mostly found in the marginal ice zone). The class 'open water' included the two subclasses open water with high and very high wind speed conditions and a third subclass that represented a mixture of calm open water, frazil ice, leads and nilas. These manual classification results were collocated with texture feature images (description provided in Sect. 3.4 and 4.2) to get a number of training vectors. For the final product the subclasses were merged into the main classes 'sea ice' and 'open water' since the similarities between the subclasses are too high for a reliable discrimination without additional data.

### 25 3.4 Calculation of texture features

The calculation of texture features consists of the computation of the gray level co-occurrence matrix (GLCM) using Eq. (1) and the calculation of texture features based on the GLCM (Equations 2 – 9). Considering the full range of possible brightness levels (e.g. 0 – 255) and a small window size most GLCM elements would be zero and that would have a negative effect on the classification result. Therefore we divide the full range into few intervals (quantization levels  $K$ ). The GLCM is created for each direction  $\theta$ , where each cell  $(i, j)$  is a measure of the relative frequency of two pixels occurrence with brightness  $i$  and  $j$  respectively, separated by a co-occurrence distance  $d$ . One may also say that the matrix element  $P_{d,\theta}(i,j)$  is a

measure of the second order statistical probability for changes between gray levels  $i$  and  $j$  at a particular displacement distance  $d$  and at a particular angle (direction)  $(\theta)$ . The size of square GLCM is equal to number of quantized brightness levels  $K$ . The GLCM is averaged over four directions  $\theta$  ( $0^\circ$ ,  $45^\circ$ ,  $90^\circ$ ,  $135^\circ$ ) to account for possible rotation of the ice floes (Clausi, 2002).

$$S_{d,\theta}(i, j) = \frac{P_{d,\theta}(i, j)}{\sum_{i=1}^K \sum_{j=1}^K P_{d,\theta}(i, j)} \quad (1)$$

where  $S_{d,\theta}$  – GLCM,  $P_{d,\theta}$  – number of neighbor pixel pairs,  $\theta$  – fixed vector directions ( $0^\circ$ ,  $45^\circ$ ,  $90^\circ$ ,  $135^\circ$ ),  $d$  – co-occurrence distance,  $K$  – number of quantized gray levels,  $i, j$  – gray levels ( $0 - 255$ ).

$$Energy = \sum_{i=1}^K \sum_{j=1}^K [S_{d,\theta}(i, j)]^2, \quad (2) \quad Homogeneity = \sum_{i=1}^K \sum_{j=1}^K \frac{S_{d,\theta}(i, j)}{1 + (i - j)^2}, \quad (3)$$

$$Contrast = \sum_{i=1}^K \sum_{j=1}^K (i - j)^2 S_{d,\theta}(i, j), \quad (4) \quad Correlation = \frac{\sum_{i=1}^K \sum_{j=1}^K (i - \mu_x)(j - \mu_y) S_{d,\theta}(i, j)}{\sigma_x \sigma_y}, \quad (5)$$

$$Entropy = - \sum_{i=1}^K \sum_{j=1}^K S_{d,\theta}(i, j) \log_{10} S_{d,\theta}(i, j), \quad (6) \quad Kurtosis = \sum_{i=1}^K \sum_{j=1}^K \frac{(S_{d,\theta}(i, j) - \mu)^4}{\sigma^4}, \quad (7)$$

$$Skewness = \sum_{i=1}^K \sum_{j=1}^K \frac{(S_{d,\theta}(i, j) - \mu)^3}{\sigma^3}, \quad (8)$$

$$ClusterProminence = \sum_{i=1}^K \sum_{j=1}^K (i + j - \mu_x - \mu_y)^4 S_{d,\theta}(i, j), \quad (9)$$

where  $\sigma_x^2 = \sum_{i=1}^K \sum_{j=1}^K (j - \mu_x)^2 S_{d,\theta}(i, j)$  and  $\sigma_y^2 = \sum_{i=1}^K \sum_{j=1}^K (j - \mu_y)^2 S_{d,\theta}(i, j)$  are standard deviation of rows and columns;

$\mu_x = \sum_{i=1}^K \sum_{j=1}^K i S_{d,\theta}$  and  $\mu_y = \sum_{i=1}^K \sum_{j=1}^K j S_{d,\theta}$  are mean values of rows and columns;  $\sigma^2 = \sum_{i=1}^K (i - \mu)^2 \sum_{j=1}^K S_{d,\alpha}(i, j)$  - standard deviation

$$\text{and } \mu = \sum_{i=1}^K \sum_{j=1}^K i S_{d,\alpha}(i, j) \text{ - mean values of brightness.} \quad (10)$$

The results of this procedure depend on several factors such as the size of the sliding window, the co-occurrence distance, and the quantization levels (Shokr, 1991; Soh and Tsatsoulis, 1999; Clausi, 2002). In order to test the effects of these parameters on the classification accuracy, texture features were calculated for the window sizes 16, 32, 64, and 128 pixels using different co-occurrence distances and varying the number of quantized gray levels (Table 1). The optimal values for the parameters of texture features calculation were selected analysing variations in the texture parameters by the visual estimation of the normalized mean values distribution of each texture feature for defined class. The decision is made for the benefit of the cases when the separation of the normalized texture values for the classes increases in the majority of investigated texture feature figures. Defined parameters were applied for calculations of all set of texture features, and then the visual comparison showed the best discrimination between the ice \ water classes for some texture features (details provided in Sect. 4.2).



A selection procedure is applied to limit a set of texture characteristics that provides a good classification with a small computational load. This procedure includes visual assessment of scatterplots comparing values of texture features in different combinations. Candidate texture features that provide the best separation of classes are selected and others are discarded. The selection procedure also uses a set of training image regions to establish the set of features and its computation parameters providing the smallest classification error. In other words, we constrain the texture features number by the demanded balance considering the SAR image level of details, computation time and the optimal reliable class separation.

### 3.5 Support Vector Machines

The Support Vector Machines are supervised learning methods with associated learning algorithms that provide data classification. The basic SVM takes a set of input data (several “attributes”, i.e. the features or observed variables) and predicts (i.e. the class labels) for each given input, which forms the output, making it a non-probabilistic classifier. The support-vector network maps the input vectors into a high dimensional feature space through non-linear mapping. SVM finds a linear hyperplane separating objects into classes by the most widely clear gap between the nearest training data points of any class. An optimal hyperplane is defined as the linear decision function with maximal margin between the vectors in this higher dimensional space. When the maximum margin is found, only points which lie closest to the hyperplane have weights  $> 0$ . These points determine this margin and are called support vectors (Cortes and Vapnik, 1995).

SVM performs a non-linear classification using the kernel trick. The kernel function may transform the data into a higher dimensional space to make this nonlinearly separation possible when the relation between class labels and attributes is nonlinear. A common choice is a Gaussian kernel. In our study we have used the radial basis function kernel (RBF kernel), which is found to work well in a wide variety of applications.

The scikit-learn open source was used to implement the SVM classification method. SVM models derived from LIBSVM software, which is applied in scikit-learn. Basically, SVM trains the model using low-level method and can only solve binary classification problems. In the case of multi-class classification, LIBSVM implements the “one-against-one” technique by fitting all binary sub-classifiers and finding the correct class by a voting mechanism. The effectiveness of SVM training depends on the selection of kernel, the kernel's parameters ( $\gamma$ ), and margin parameter C. The software provides a simple tool to check a grid of parameters obtaining cross-validation accuracy for each parameter setting. Finally, the parameters with the highest cross-validation accuracy are returned (Hsu et al., 2003). SVM parameters in our case were taken:  $\gamma=1$ ,  $C=1$ .

The calculated texture features and  $\sigma^\circ$  values corresponding to the manually identified classes on several pre-processed RS2 images were used as input data for training the SVM classifier. After completing the training procedure, the resulting SVM is used for automatic sea ice classification.

### 3.6 Validation

Validation of Arctic sea ice classification results is a challenging task since sea ice is a very inhomogeneous medium and validation data on ice classification is difficult to obtain. As a substitute our sea ice classification results have been compared with manual sea ice charts produced by the operational ice service at the Norwegian Meteorological Institute (MET Norway, <http://polarview.met.no/>). MET Norway produces ice charts every work day using the following data sources: high resolution SAR images, low resolution microwave SSM/I and SSMIS data (DMSP), MODIS images (Terra and Aqua) and AVHRR data from NOAA. In our comparison MET Norway ice charts are assumed to represent “true” classification and the confusion matrix was calculated for accuracy evaluation of our algorithm results.

### 4 Results

To illustrate the algorithm performance the automatic SVM classification was applied to the RS2 scene shown in Figure 2. The example scene was acquired on November 28, 2011 over the western part of Svalbard in Fram Strait. Figure 2 and 3 show both HH and HV polarizations before and after corresponding corrections described in Sect. 2: compensation of incidence angle effects for HH (Fig. 3a) and noise reduction for HV (Fig. 3b). The image contains several ice types, open water under different wind conditions and land. The open water area is located on the right-hand side of the image and the ice-covered area - in the upper-left corner. The sea ice area includes a marginal ice zone with bright broken up ice. The ice-covered areas and the rough OW areas appear both bright in HH and are therefore difficult to distinguish. Including HV, however, provides additional information since OW areas on this image appear generally darker than sea ice in HV. This is one of the major dual polarization advantages and can be seen in the lower right part of the example image (Fig. 2).

#### 4.1 Correction for incidence angle and thermal noise

The linear trend coefficient used for backscatter angular dependence correction of HH was estimated to be  $-0.298\text{db/1}^\circ$  and allowed normalization of  $\sigma^\circ$  to the incidence angle  $35^\circ$  as shown on Figure 3 a and c. The application of our noise correction procedure for HV reduces significantly thermal noise and get rid of vertical striping as shown in Fig. 3b, d.

#### 4.2 Texture features calculation

As part of the algorithm development texture features were calculated based on different parameter settings. Visual examination of mean values of several texture features (Fig. 4a, b) suggested the optimal combination of the sliding window, moving step and distance between neighbouring pixels which provides better separation of the ice / water classes compared to other combinations of window sizes with different texture parameters. A set of texture characteristics was selected analysing variations in mean values of the textural characteristics of defined classes calculated with several combinations of obtained parameters (Fig. 4c, d). The largest change of distance between mean values of texture features of different classes on Figure 4d defines the best option for the potential classification. Finally, together with visual inspection of the texture

images (some examples are given on Fig. 5a – f) of the a priori known most problematic classification cases on the SAR images used for training, the set of texture characteristics are defined. The best results were achieved using the following parameter set: number of gray levels  $K=32$ , co-occurrence distance  $d=8$ , sliding window size  $w=64 \times 64$ , moving step of the sliding window  $s=16$ . Using the following texture features for the two channels provided the best test results: HH - energy, inertia, cluster prominence, entropy, 3rd statistical moment of brightness, backscatter, and standard deviation; HV - energy, correlation, homogeneity, entropy, and backscatter. Including more texture features for both channels was tested but found not to improve the information content. The calculation parameters were found experimentally to give a good compromise between speckle noise reduction, preservation of details and correct classification results [methodology description in Zakhvatkina et al., 2013].

Texture characteristics provide a more complete delineation of surface parameters in addition the raw backscatter signal and increase the ability for ice and water separation. The scatterplots in Fig. 5g, h show the values of two different texture features plotted against each other and illustrate the usefulness of texture features for discrimination between defined classes.

### 4.3 Manual versus automatic classification

As described in Sect. 3 several SAR images were classified manually as part of the training procedure for the automatic algorithm. Comparing the manual classification from sea ice expert analysis with the algorithm results (Fig. 6) reveals a general high level of correspondence and illustrates the capability of the automatic approach. Detailed observation of the classification results show that most misclassifications are observed near land and in the MIZ. Fig. 6b shows small features inside ice-covered zone (blue dots) that were misclassified as OW.

### 4.4 Validation

Validation of the algorithm results has been performed using 2705 RS2 images taken over our area of interest in the period 1 January 2013 until 25 October 2015. For each RS2 image an error matrix based on pixel-by-pixel difference between algorithm result and MET Norway chart has been calculated. OW and sea ice correspondence as well as an overall accuracy were obtained for each RS2 image classification result and averaged accuracies have been calculated for each month. The impact of each class on the classification error has been estimated and the respective monthly averaged errors were computed. The averaged overall accuracies including standard deviation and errors in ice and water classification for each month are given in Table 2. In addition, the monthly accuracies are presented as a graph in Fig. 7. The monthly averaged overall accuracies show lower values during summer months (Fig. 7 - from May to October) and higher values during winter. The average total classification accuracy for all 2705 scenes is  $91 \pm 4 \%$ .

Figure 8 shows an example of the validation process. The RS2 HH image is shown in Figure 8a, the result of our SVM classification in Figure 8c and the MET Norway sea ice chart in Figure 8b. To compare the algorithm result with the manually derived ice charts, both products are reclassified into ice and water (Figure 8d and 8e). The error matrix is

represented as an image (Figure 8f) with the following three classes: no difference; sea ice error (sea ice at MET Norway, OW at our results); OW error (OW at MET Norway, sea ice at our results).

## 5 Discussion

### 5.1 Significance of incidence angle variations and thermal noise reduction

5 Water areas have a very large range of brightness depending on wind speed. At higher wind speeds the contrast between open water and sea ice is reduced, which gives an ambiguity between these classes. The dependence of backscatter on incidence angle is well known (Shokr, 2009) and is significantly higher for open water than for sea ice. The correction factor for the incidence angle is therefore very different for ice and water. Coefficients for angular dependence of water covered areas are significantly influenced by wind conditions - with stronger wind intensity grows faster. Our observations show that angular dependence of sea ice is more stable regardless of wind or other conditions. Since the surface type is not known a priori, we have to choose which angular correction to apply and the preference is given to the more reliable sea ice angular correction. However, the total compensation is impossible as the backscatter dependence on the incidence angle varies for different ice types (Makynen et al, 2002) and water areas on the one scene. The radiometric corrections during calibration process are just a first-order approximation; nevertheless, the advantages of performing the angular correction are greater than the disadvantages (Moen et al., 2015). With regards to thermal noise correction, we can observe that sometimes not all visible noise floor artifacts inside beams can be completely removed and these residuals may cause classification errors.

### 5.2 Number of texture features vs efficiency

In addition to the 8 extracted texture features we characterize the surface by values of  $\sigma^\circ$  averaged within the sliding window and a value of standard deviations. Given that we have two channels (HH and HV) the number of parameters grows up to 20 and some of them are strongly intercorrelated (Shokr, 1991; Albrechtsen, 2008). High correlation between two textural characteristics shows the similar properties of the classes and it makes no sense of using both features. In case of low correlation both features will contribute to the improvement of the classification accuracy (Clausi, 2002). This similarity can explain the misclassifications and in fact this is part of the motivation to reduce dimensionality. If we include too few texture features to the classifier then the informationally poor features have to be compensated by using complicated discrimination function and can lead to increased classification confusion. On the other hand, if all texture features are used by the classifier, some classes can be underestimated or overestimated and the discrimination for many classes may lead to higher classification errors.

Sea ice in upper part of Fig. 5a could not be distinguished from rough open water (upper right). However, Fig. 5b shows reliable detection of sea ice-covered area (left side). Open water calm can be easily distinguished on Fig. 5c, whereas Fig. 5d provides additional information about OW calm location (dark blue colored area). The same situation is shown on Fig. 5d – a border between heterogeneous sea ice area and open water area (the bright colored ice), which consist of very close ice floes

and/or broken ice, has the highest values (Fig. 5d) and is clearly seen, but some other ice-covered area can be incorrectly defined as open water. Figure 5e adds more useful information about open water location (blue colored area). The scatterplot on Fig. 5g, h represents advantage of texture feature application for discrimination between the sea ice and two classes of open water using both polarizations, where sea ice (green) can be clearly seen as standing separately from OW (blue). The scatterplot in Fig. 5h demonstrates how different texture characteristics, e.g. energy versus correlation, of different polarizations can add useful information for detection. The examples in Fig. 5e and f show that the same texture feature calculated for one polarization can be used in applications to obtain well-delineated class, otherwise for other polarization it demonstrates the poor separation between classes.

### 5.3 Sources of errors

The MET Norway manual products and our algorithm results show generally a good consistency. However, differences typically appear at the ice – water boundary and inside ice-covered areas, where leads or channels on the SAR image are not delineated on the MET Norway ice charts. Some differences are also found in the coastal zones, where narrow ice zones near the coast are wrongly shown in our results or fast ice is wrongly classified as OW by our algorithm. This misclassification can be explained by appearance of fast ice and calm open water on a SAR image and its similarity in the low backscatter. For this case the polarization difference in backscatter between HH and HV bands (cross-polarization ratio) could be included for further improvement (Sandven, 2008; Dierking and Pedersen, 2012; Moen et al., 2013). More significant classification errors can be found in the MIZ. This area is particularly difficult to classify automatically due to its very smooth ice signature.

Detecting typical backscatter ranges and textural structures for different sea ice types and water areas with different roughness stages is extremely difficult due to the high dynamic and variable nature of sea ice and wind speed impact. In particular, different structures on the water affected by wind and currents and visually detected on the SAR images (e.g. stripes, eddies, etc.) may cause wrong sea ice classification.

Residual HV noise effects (after correction) along the ScanSAR image beam boundaries and false signal variations inside the separate beams (Fig. 5b, d) can have an uncorrected effect on the texture feature analysis and may cause classification errors. These residual noise effects are not visible in the ice-covered areas, but rough open water on high incidence angle close to the beam boundaries may be erroneously classified as sea ice.

The backscatter signal of melting ice becomes similar to open water and imposes limitations for the classification of RS2 images for the summer season.

We assume that our automatic algorithm classifies SAR images more reliable than represented by the provided accuracy (91%), and this inconsistency may occurs for the following reasons:

1) Different resolution and disagreements in interpretation: The MET Norway ice charts have a lower resolution than our automatic ice charts making an absolute accurate estimation the ice conditions in the each SAR images and detailed comparison impossible.

- 2) Different classes: The classes obtained by MET Norway are not consistent with the simple ice water classification provided by the algorithm. In the comparison, we reclassify the MET Norway ice chart into ice and open water using a threshold of 10%. This assumption appears to be the subjective error factor during the validation process and finally reduces the accuracy.
- 5 3) Different timing: MET Norway provides manual ice charts for every working day, but not for weekends and holidays. This might cause a difference in timing up to several days. Manual and automatic ice charts of the same day might also not be based on images taken at the same time of the day. Fram Strait is a very dynamic region and the sea ice situation can significantly change over time periods of several hours.

## 6 Conclusion

- 10 We have proposed an automated OW / ice cover classification of RADARSAT-2 SAR ScanSAR Wide beam mode data acquired over Fram Strait during different wind speed and sea ice conditions. The classification uses backscatter and texture features together in a SVM approach. Higher wind speed increases the contrast of open water area on different polarizations (HH and HV) and the water is distinguished more reliably on dual-polarized RS2 data.
- Previous studies of ENVISAT ASAR HH data in Wide Swath Mode showed a similar backscatter dependence on incidence
- 15 angle (Zakhvatkina et al., 2013), and the same technique was applied for HH-band of RS2 SCW images. The ScanSAR image swath consists of different combinations of four physical beams and there are well-known technical features caused by a wave-like modulation of the image intensity in azimuth direction throughout the entire image in the sub-swaths and their edges of HV band (Romeiser et al, 2010). Although the techniques for compensating the effect in the SAR processor have been developed and applied, some ScanSAR images are still showing residual effects. To improve utilization of such
- 20 images we have carried out a procedure of HV band noise reduction that is applied as a pre-processing tool. By computing texture features with sliding window size of  $64 \times 64$  pixels and number of quantized gray levels amounted 32, we classified more that 2700 SAR images for the period from January, 2013 to October, 2015. Validation of the classification was done by comparing with ice charts produced by MET Norway. The results show that SVM texture algorithm discriminated between open water and sea ice areas with accuracy 91%.
- 25 The automated SVM based algorithm has been adopted for operational decoding of open water and ice boundary, and it will also be extended and improved for sea ice type classification (Korosov, 2016). With Sentinel- 1A/B as the main satellite SAR system in the coming years, the next step will be to adapt the classification algorithm to Sentinel-1 data. The amount of SAR data available for sea ice monitoring will increase significantly in the coming years. Efficient utilization of these data will require further efforts to develop automated algorithms which can be used in operational ice services.



## Acknowledgements

The work has been supported by the EU projects MyOcean (Grant agreement no. 218812), SIDARUS (Grant agreement no. 262922), MAIRES (Grant agreement no. 263165), Research Council of Norway (contract 196214), Norwegian Space Center (JOP.01.11.2), and EuRuCAS (Grant agreement no. 295068), SONARC project under Research Council of Norway (contract no 243608) and Russian Foundation for Basic Research (RFBR) project SONARC (Grant agreement no. 15-55-20002). We acknowledge the MDA for providing RADARSAT-2 data through SIDARUS project. Authors would thank Nick Hughes from Norwegian Meteorological Institute for providing high resolution ice charts for validation of the classification method.

## References

- Albregtsen, F.: Statistical Texture Measures Computed from Gray Level Cooccurrence Matrices, Image Processing Laboratory Department of Informatics University of Oslo, November 5, 2008.
- Bogdanov, A. V., Sandven, S., Johannessen, O. M., Alexandrov, V. Y., and Bobylev, L. P.: Multisensor approach to automated classification of sea ice image data, *IEEE T. Geosci. Remote*, 43, 1648-1664, 2005.
- Clausi, D. A.: An analysis of co-occurrence texture statistics as a function of grey level quantization, *Can. J. Remote Sens.*, 28, 45 – 62, 2002.
- 15 Clausi, D.A., Qin, A.K., Chowdhury, M.S., Yu, P., and Maillard, P.: MAGIC: MAP-Guided Ice Classification System, *Can. J. Remote Sens.*, 36, suppl. 1, S13–S25, 2010.
- Cortes, C. and Vapnik, V.: Support-Vector Networks, *Machine Learning*, 20, 273-297, 1995.
- Dierking, W.: Mapping of different sea ice regimes using images from Sentinel-1 and ALOS synthetic aperture radar, *IEEE T. Geosci. Remote*, 48, 1045–105, 2010.
- 20 Dierking, W. and Pedersen, L.: Monitoring sea ice using ENVISAT ASAR— A new era starting 10 years ago, in *Proc. IEEE Int. Geosci. Remote SE (IGARSS2012)*, 1852–1855, 2012.
- Dierking, W.: Sea ice monitoring by synthetic aperture radar, *Oceanography*, 26, 100–111, 2013.
- Dokken, S.T., Markus, P.W.T., Askne, J., and Bjork, G.: ERS SAR characterization of coastal polynyas in the Arctic and comparison with SSM/I and numerical model investigations, *Remote Sens. Environ.*, 80, 321–335, 2002.
- 25 Geldsetzer, T., and Yackel, J. J.: Sea ice type and open water discrimination using dual co-polarized C-band SAR, *Can. J. Remote Sens.*, 35 , 73–84, 2009.
- Gill, R.S.: SAR Ice Classification Using Fuzzy Screening Method, in *Proc. Workshop on Applications of SAR Polarimetry and Polarimetric Interferometry (POLinSAR)*, 14-16 January 2003, Frascati, Italy.
- Gill, J.P.S., and Yackel, J.J.: Evaluation of C-band SAR polarimetric parameters for discriminating of first-year sea ice types, *Can. J. Remote Sens.*, 38, 306–323, 2012.
- 30 Haarpaintner, J. and Solbø, S.: Automatic ice-ocean discrimination in SAR imagery, Norut IT-report, Tech. Rep., 2007.

- Haralick, R. M., Shanmugam, K. S., and Dinstein, I.: Textural features for image classification, *IEEE T. Syst. Man. Cyb.*, 3, 610–621, 1973.
- Hsu, C.-W., Chang, C.-C., Lin., C.-J.: A practical guide to support vector classification. Initial version: 2003. Last updated: May 19, 2016. Available: <http://www.csie.ntu.edu.tw/~cjlin/papers/guide/guide.pdf>.
- 5 Jefferies, B.: Radarsat-2—New Ice Information Products, *Proc. of the 13th Meeting—International Ice Charting Working Group*, 15–19 October 2012, Tromso, Norway.
- Johannessen, O. M., Alexandrov, V., Frolov, Bobylev L., Sandven, S., Miles, M., Pettersson, L., Kloster, K., Smirnov, V., Mironov, Y., and Babich, N.: *Remote Sensing of Sea Ice in the Northern Sea Route: Studies and Applications*. Chichester, U.K.: Springer-Praxis, 2007.
- 10 Karvonen, J., Simila, M., and Makynen, M.: Open Water Detection from Baltic Sea Ice Radarsat-1 SAR Imagery, *IEEE T. Geosci. Remote Lett.*, 2, 275-279, 2005.
- Karvonen, J.: C-band sea ice SAR classification based on segmentwise edge features, in *Geoscience and Remote Sensing New Achievements*, P. Imperatore, and D. Riccio, Ed., In- Tech, 129 – 146, 2010.
- Karvonen, J.: Operational SAR-based sea ice drift monitoring over the Baltic Sea, *Ocean Sci.*, 8, 473–483, 2012.
- 15 Korosov, A., Hansen, M. W., and Yamakava, A.: Nansat – scientist friendly toolbox for processing satellite data, *World Ocean Scientific Congress*, 2–8 February, 2015, Cochin, India.
- Korosov, A.: Very high resolution classification of Sentinel-1A data using segmentation and texture features, *Proc. of European Space Agency Living Planet Symposium*, 9-13 May 2016, Prague, Czech Republic.
- Leigh, S., Zhijie, W., and Clausi, D.A.: Automated Ice–Water Classification Using Dual Polarization SAR Satellite Imagery, *IEEE T. Geosci. Remote*, 52, 5529 -5539, 2014.
- 20 MacDonald Dettwiler and Associates (MDA): RADARSAT-2 product description, *Tech. Rep. Issue 1/8*, April 15, 2011. Available: [http://gs.mdacorporation.com/includes/documents/RN-SP-52-1238%20RS-2%20Product%20Description%201-8\\_15APR2011.pdf](http://gs.mdacorporation.com/includes/documents/RN-SP-52-1238%20RS-2%20Product%20Description%201-8_15APR2011.pdf) (last access: 1 July 2014).
- Maillard, P., Clausi, D.A., and Deng, H.: Map-guided sea ice segmentation and classification using SAR imagery and a MRF segmentation scheme, *IEEE T. Geosci. Remote*, 43, 2940–2951, 2005.
- 25 Mäkynen, M. P., Manninen, A. T., Similä, M. H., Karvonen, J. A., and Hallikainen, M. T.: Incidence angle dependence of the statistical properties of C-band HH-polarization backscattering signatures of the Baltic Sea ice, *IEEE T. Geosci. Remote*, 40, 2593–2605, 2002.
- Moen, M.-A. N., Doulgeris, A. P., Anfinsen, S. N., Renner, A. H. H., Hughes, N., Gerland, S., and Eltoft, T.: Comparison of automatic segmentation of full polarimetric SAR sea ice images with manually drawn ice charts, *The Cryosphere.*, 7, 2595–2634, 2013.
- 30 Moen, M.-A.N., Anfinsen, S.N., Doulgeris, A.P., Renner, A.H.H., and Gerland S.: Assessing polarimetric SAR sea-ice classifications using consecutive day images, *Ann. Glaciol.*, 56(69), 285 – 294. 2015.

- Ochilov, S. and Clausi, D. A.: Operational SAR sea-ice image classification, *IEEE T. Geosci. Remote*, 50, 4397 – 4408, 2012.
- Romeiser, J. Horstmann, Caruso, M.J., and Graber, H.C.: A descalloping post-processor for ScanSAR images of ocean scenes, *IEEE T. Geosci. Remote*, 51, 3259-3272, 2013.
- 5 Sandven, S., Kloster, K., Alexandrov, V., and Piotrovskaya, N. [Zakhvatkina]: Sea ice classification using ASAR Alternating Polarisation images, *SeaSAR 2008*, 21 -24 January 2008, Oslo, Norway.
- Sandven, S., Alexandrov, V., Zakhvatkina, N., and Babiker, M.: Sea ice classification using RADARSAT-2 Dual Polarisation data, *SeaSAR 2012*, the 4th International Workshop on Advances in SAR Oceanography, 18 -22June 2012, Tromso, Norway.
- 10 Shokr, M. E.: Evaluation of Second-Order Texture Parameters for Sea Ice Classification from Radar Images, *J. Geophys. Res.*, 96, 10625–10640, 1991.
- Shokr, M. E.: Compilation of a radar backscatter database of sea ice types and open water using operational analysis of heterogeneous ice regimes: *Can. J. Remote Sens.*, 35, 369–384, 2009.
- Soh, L.K. and Tsatsoulis, C.: Texture analysis of SAR sea ice imagery using gray level co-occurrence matrices, *IEEE T. Geosci. Remote*, 37, 780–795, 1999.
- 15 Soh, L. K., Tsatsoulis, C., Gineris, D., and Bertoia, C.: ARKTOS: An intelligent system for SAR sea ice image classification, *IEEE T. Geosci. Remote*, 42, 229–248, 2004.
- Unser, M.: Sum and difference histograms for texture classification, *IEEE T. Pattern Anal.*, 8, 118–125, 1986.
- Vinje, T. and Finnekåsa, Ø.: The ice transport through the Fram Strait. *NorskPolarinstituttSkrifter* 186, 39, 1986.
- 20 Yu, Q. and Clausi, D. A.: IRGS: Image segmentation using edge penalties and region growing, *IEEE T. Pattern Anal.*, 30, 2126–39, 2008.
- Yu, P., Qin, A. K., and Clausi, D.A.: Feature extraction of dual-pol SAR imagery for sea ice image segmentation, *Can. J. Remote Sens.*, 38, 352-366, 2012.
- Zakhvatkina, N., Alexandrov, V., Johannessen, O. M., Sandven, S., and Frolov, I.: Classification of sea ice types in  
25 ENVISAT synthetic aperture radar images, *IEEE T. Geosci. Remote*, 51, 2587–2600, 2013.

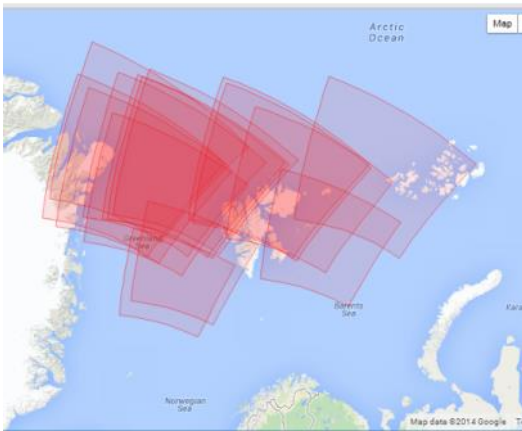


**Figure 1. Location of RADARSAT-2 image used for training. All data are provided in GeoTIFF format with auxiliary XML files by Center for Earth Observation and Digital Earth (CEODE).**

5

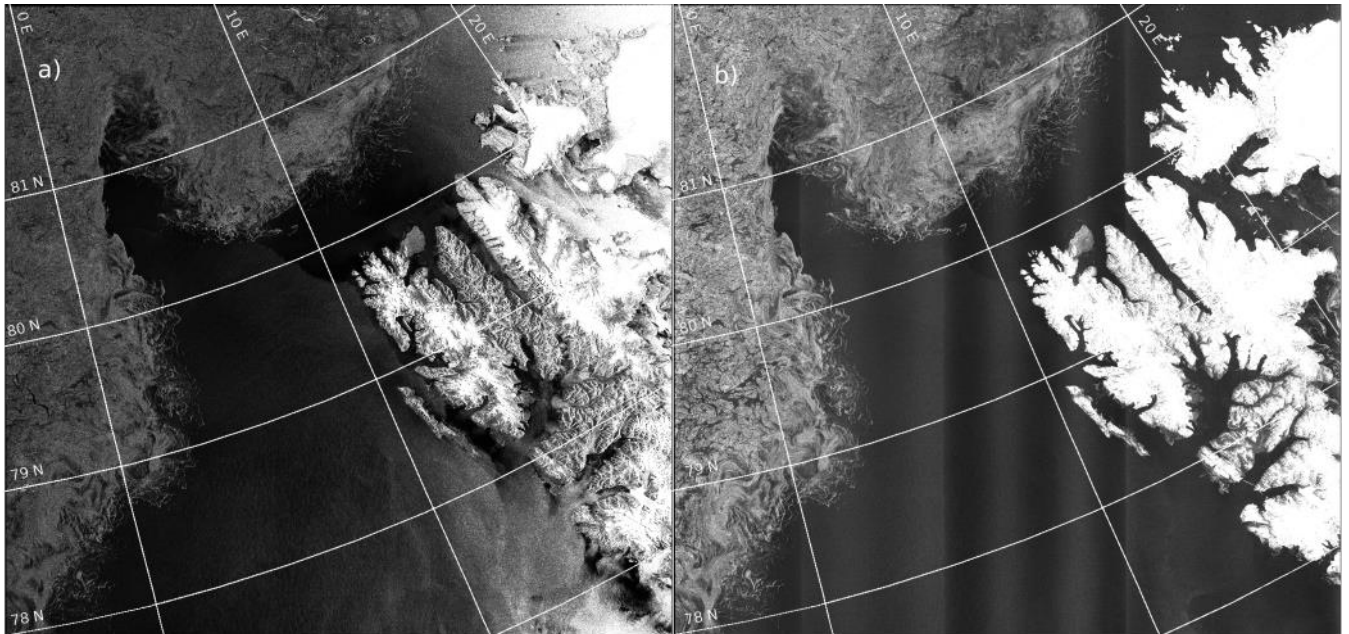


**Figure 2. RS2 SCWA dual-polarization image taken over Fram Strait on November 28, 2011 prior pre-processing. a) HH channel with angular dependence; b) HV channel with along track noise floor variations.**

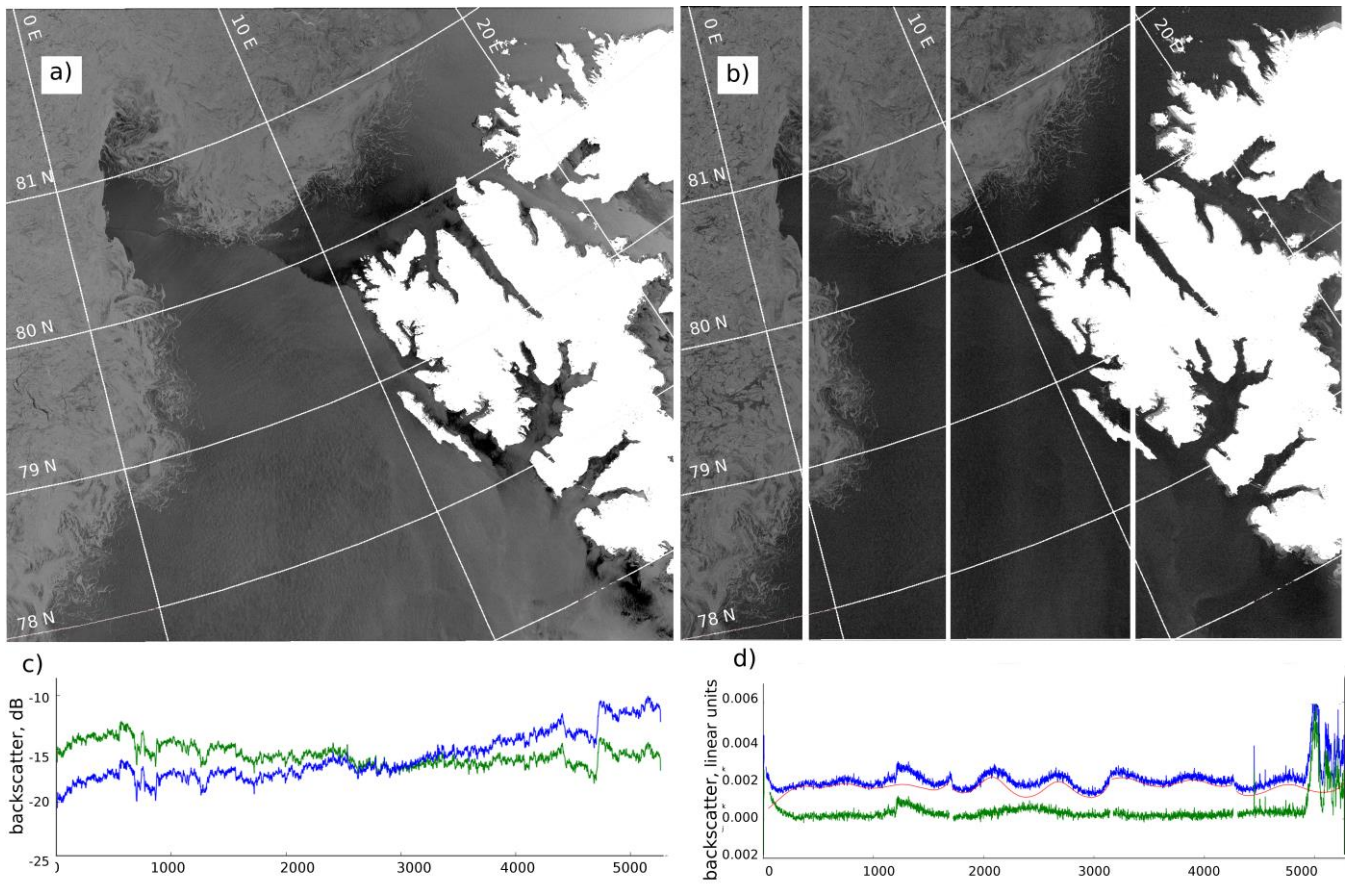


Figure 3. RS2 SCWA dual-polarization image taken over Fram Strait on November 28, 2011 including pre-processing. a) Calibrated image after correction of  $\sigma^0$  at  $35^\circ$  incidence angle using predefined coefficient for sea ice=  $-0.298\text{db}/1^\circ$ ; b) Noise corrected image: beam boundaries are visible due to differences in noise levels between adjacent beams; c)  $\sigma^0$  curves of SAR image across the entire swath: original image (blue) and after angular correction (green); d)  $\sigma^0$  curves of SAR image along the whole swath. The blue curve shows  $\sigma^0$  value profile of the raw HV channel image over the horizontal line, the red curve depicts the noise floor level and the green curve is the result of subtraction.

Table 1. Experiments of computation parameters:

$W$	$d$	Moving step	$K$
32	4	8/16/32	16/25/32
32	8	8/16/32	16/25/32
32	16	8/16/32	16/25/32
64	4	8/16/32/64	16/25/32
64	8	8/16/32/64	16/25/32
64	16	8/16/32/64	16/25/32
64	32	8/16/32/64	16/25/32
128	4	32/64/128	16/25/32
128	8	32/64/128	16/25/32
128	16	32/64/128	16/25/32
128	32	32/64/128	16/25/32
128	64	32/64/128	16/25/32

$W$  - window sizes,  $d$  - cooccurrence distances, and  $K$  -quantized grey levels, and Moving step is a step of sliding window moving.



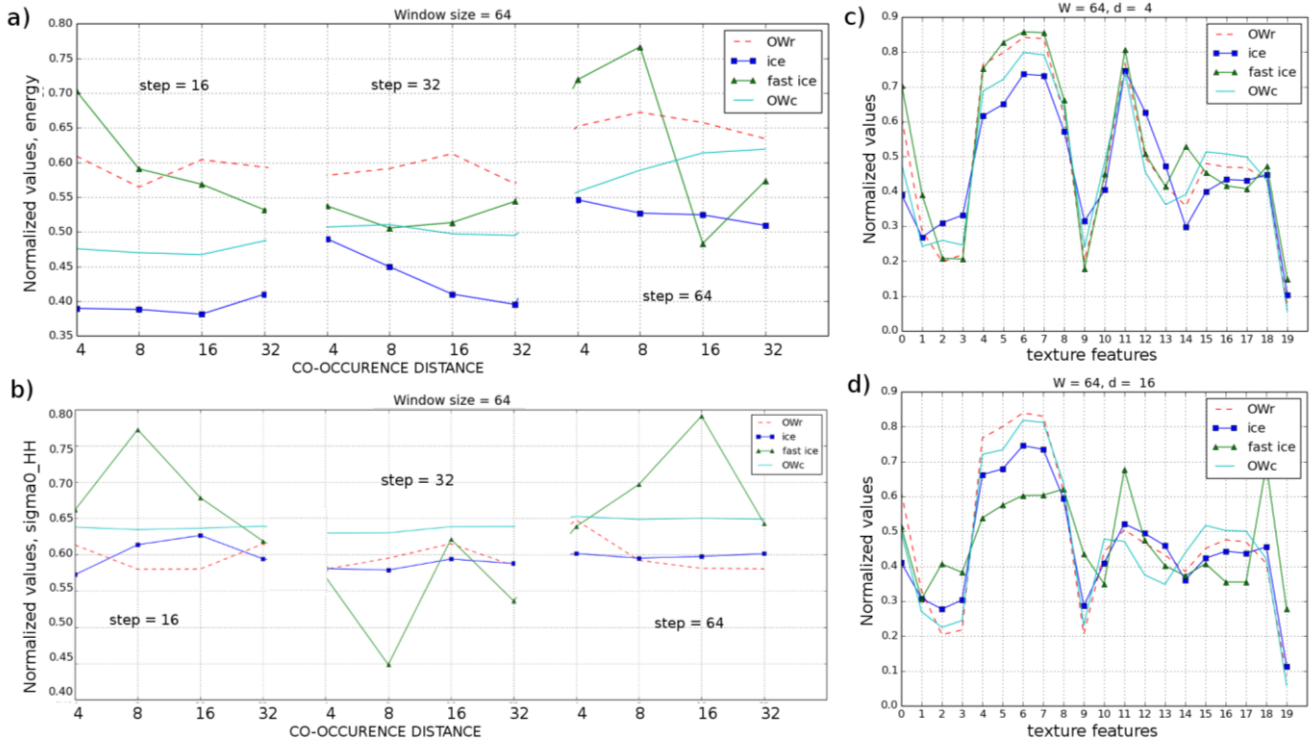


Figure 4. Normalized mean values of texture characteristics for OW calm, OW rough, ice and fast ice, calculated in window size 64x64 pixels: a) energy, and b)  $\sigma^0$  of HH with different co-occurrence distances for several moving step variations. Set of texture features are calculated with found above parameters: c) d=4 and step=16; and d) d=8 and step=16 pixels. (1 – energy, 2 – correlation, 3 – inertia or contrast, 4 – cluster prominence, 5 – homogeneity, 6 – entropy, 7 – 3rd central statistical moment of brightness, 8 – average sea ice backscatter; 9 – std of brightness) The calculations were made for several images used for training.

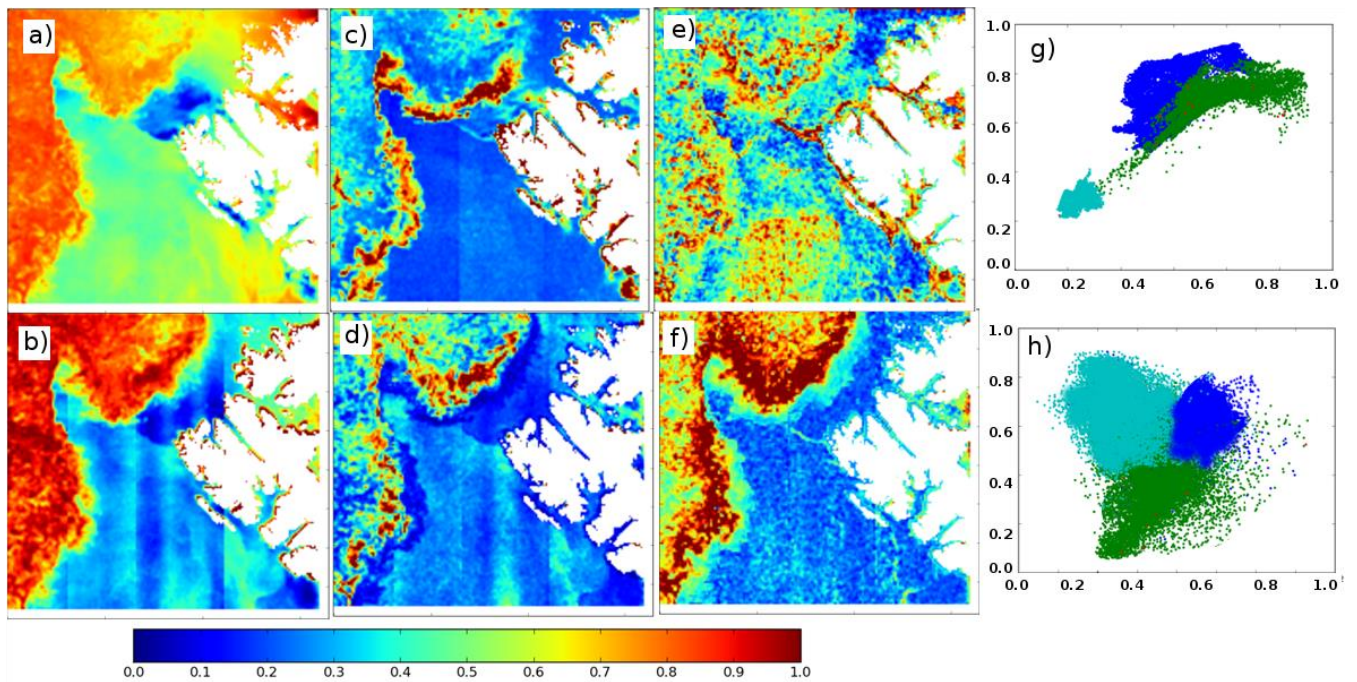


Figure 5. Texture features calculated for RS2 SCWA scene, November 28, 2011, the Fram Strait. a) Backscatter; c) Inertia; e) Correlation of HH-polarization. b) Backscatter; d) Energy; f) Correlation of HV-polarization. The scatter plots show how a couple of textural features calculated from RS2 images, shown in Fig. 1, can be used to classify ice (green), OW (blue) and calm OW (cyan). j)  $\sigma^\circ$  of HV vs  $\sigma^\circ$  of HH; h) Energy of HH vs correlation of HV.

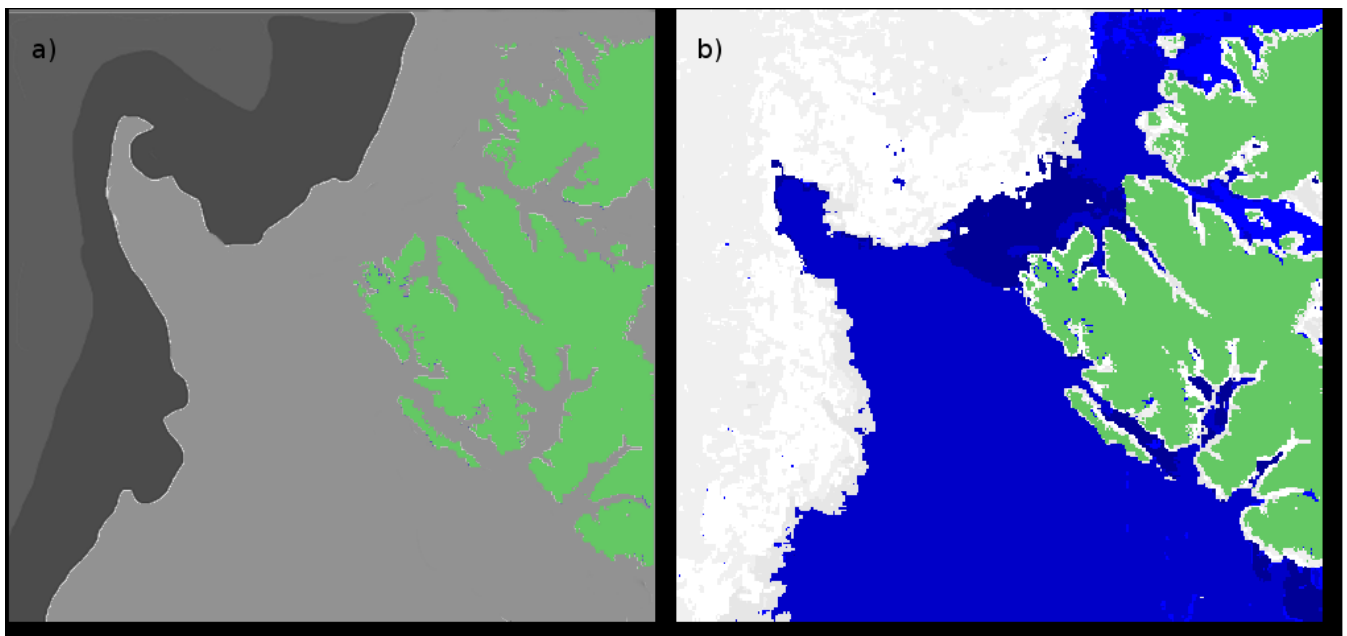


Figure 6. OW/sea ice classification of RS2 SCWA image shown in Figure 2. a) Manual classification based on sea ice expert



analysis to delineate sea ice (in the MIZ and general sea ice cover) and open water (calm and rough open water): dark gray – sea ice; very dark gray – marginal ice zone; light gray - OW; green – land. b) Automatic SVM classification result: white - sea ice; dark blue – calm OW; blue - OW; green - land.

5 Table 2. Monthly averaged accuracies of the automatic ice charts compared to MET Norway ice charts (results given in %)

2013						2014						2015					
months	images	ov acc	std	ow err	ice err	months	images	ov acc	std	ow err	ice err	months	images	ov acc	std	ow err	ice err
Jan	72	91.52	5.43	3.99	4.50	Jan	97	91.89	4.70	2.52	5.59	Jan	51	94.84	3.10	1.28	3.88
Feb	70	91.05	4.54	2.66	6.30	Feb	93	92.11	5.05	3.37	4.52	Feb	33	94.47	4.05	2.33	3.86
Mar	106	91.21	4.71	1.20	7.59	Mar	110	92.20	3.45	2.83	4.98	Mar	73	94.36	4.40	1.67	3.82
Apr	110	92.03	4.57	0.95	7.02	Apr	130	93.34	3.40	1.30	5.36	Apr	54	94.86	4.36	1.47	3.83
May	111	88.60	7.96	0.88	10.52	May	137	92.80	4.77	1.00	6.20	May	63	95.05	3.21	0.72	3.81
Jun	98	87.64	7.58	1.59	10.76	Jun	93	89.98	5.78	1.54	8.48	Jun	67	84.73	14.09	0.69	3.80
Jul	83	89.73	8.01	2.72	7.54	Jul	95	86.82	9.89	1.98	11.20	Jul	47	74.49	21.61	1.73	3.81
Aug	85	94.36	3.10	2.96	2.68	Aug	88	88.39	10.87	1.87	9.74	Aug	47	86.65	12.25	2.64	3.85
Sep	93	95.88	2.02	2.47	1.65	Sep	97	87.55	17.56	8.24	4.21	Sep	43	94.83	3.87	3.36	3.78
Okt	72	94.53	2.99	3.98	1.49	Okt	78	94.89	3.15	1.87	3.24	Okt	27	94.69	4.16	4.58	3.78
Nov	84	92.00	4.77	5.10	2.90	Nov	47	94.58	2.84	2.38	3.04	Nov					
Dec	97	90.93	6.63	3.18	5.88	Dec	54	92.94	7.99	3.45	3.61	Dec					

ovacc - monthly overall accuracy; std- standard deviation; ice err – sea ice on MET Norway ice chart, OW on automatic ice chart; OW err – OW on MET Norway ice chart, sea ice on automatic ice chart

10

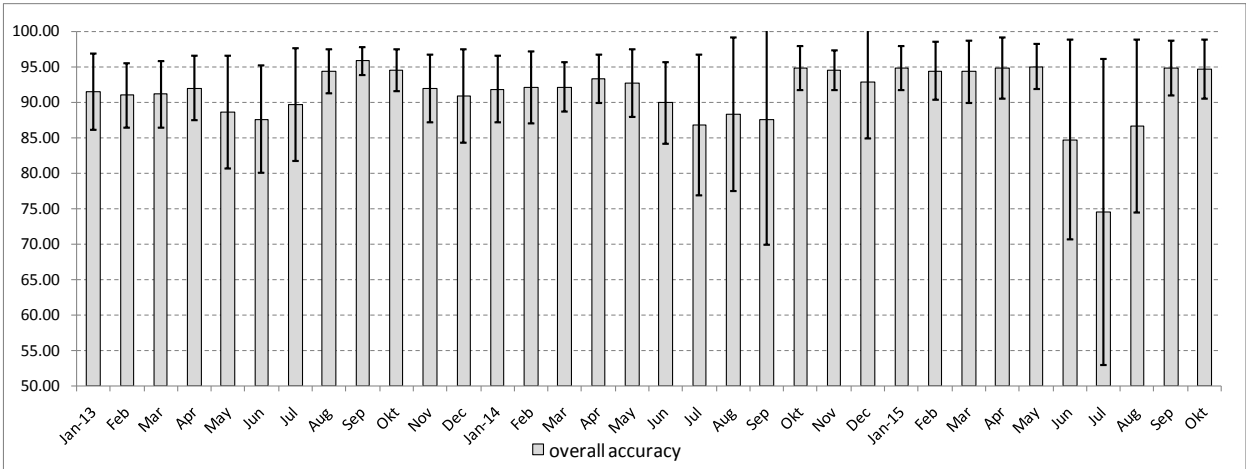


Figure 7. Monthly accuracy and standard deviation of SVM classification of RS2 images assuming that MET Norway operational ice charts are correct.

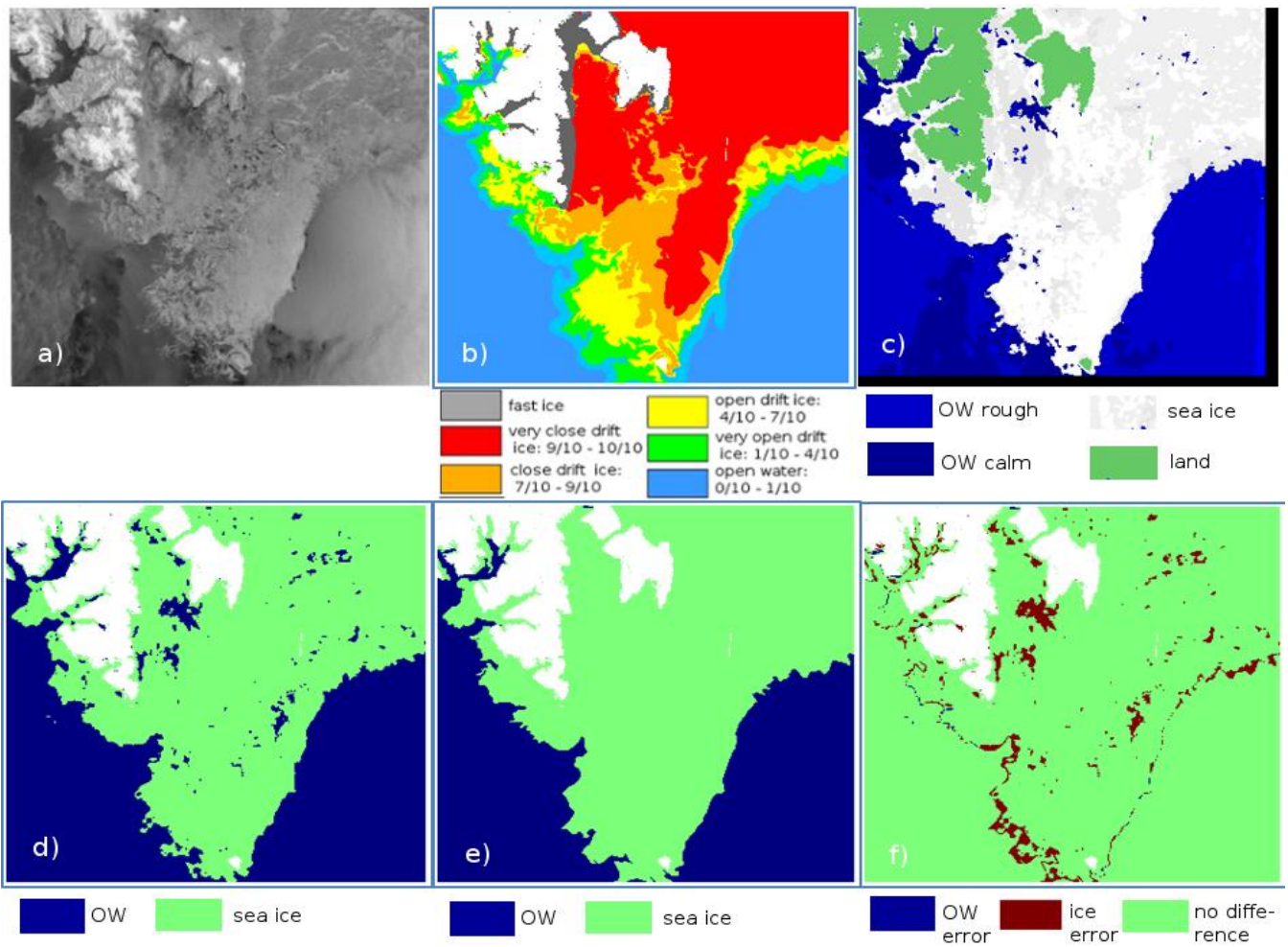


Figure 8. Validation procedure of automatic classification results compared to MET Norway ice charts. a) Original RS2 SCWA SAR image (HH-polarization), taken over the southern part of Svalbard on March 14, 2013; b) Collocated subset of manual ice concentration chart, provided by the Norwegian Ice Service (met.no) for the same day; c) Result of the SVM classification; d) Result of the SVM classification with delineation of 2 classes: water, sea ice; e) Ice chart of MET Norway reclassified into two classes: open water (ice concentration from 0 to 10%) and sea ice (ice concentration from 10% to 100%); f) Difference of recalculated MET Norway chart and classification result - represents error matrix as "image": no difference, sea ice error (sea ice at MET Norway, OW at our results), OW error (OW at MET Norway, sea ice at our results). Overall accuracy is 95.78%, OW error is 0.19%, and ice error is 4.03%.